ACS EARTH AND SPACE CHEMISTRY

Article

Cite This: ACS Earth Space Chem. 2019, 3, 599–616

http://pubs.acs.org/journal/aesccq

Kinetics of Quartz Dissolution in Natural Silicate Melts and Dependence of SiO_2 Diffusivity on Melt Composition

Yi Yu,[†] Youxue Zhang,*[,†] and Yuping Yang[‡]

[†]Department of Earth and Environmental Sciences, University of Michigan, Ann Arbor, Michigan 48109, United States

[‡]Institute of Mineral Resources, Chinese Academy of Geological Sciences, Beijing 100037, China

Supporting Information

ABSTRACT: Quartz is a major mineral in silicic rocks, and a common phenocryst in rhyolite. An understanding of the kinetics of quartz dissolution and growth may provide insight into magma crystallization and constraints on magma dynamics and cooling rates. We have carried out quartz dissolution experiments in rhyolitic (0.1 wt % H_2O, ~73 wt % SiO_2) and basaltic (~0.35 wt % H_2O, and ~50 wt % SiO_2) melts at 1300–1600 °C and 0.5 GPa using piston cylinder apparatus. The experiments constrain the interface melt compositions at quartz saturation up to 1600 °C, which depend on whether the initial melt is rhyolite or basalt. The data on silica concentration at quartz saturation in each melt are modeled and will be important for future improvement of thermodynamic models of silicate melts. In addition, the experiments provide data on SiO_2 diffusivity, which plays major roles in the kinetics and dynamics of various igneous processes, including magma mixing. SiO_2 diffusivity depends on melt composition, consistent with previous results. Combined with other data from our lab and literature, we show that ln D_{SiO_2} decreases linearly with X (= Si + Al cation mole fraction) in rhyolitic to andesitic to basaltic melts, instead of just the SiO_2 concentration. The effect of H_2O is also captured by X when H_2O is included in the cation mole fraction calculation. Each SiO_2 diffusion profile during quartz dissolution can be fit well by assuming $D_{SiO_2} = D_{X=1}\, e^{\beta(1-X)}$. Using data from our experiments, SiO_2 diffusivity during quartz dissolution in rhyolitic, andesitic, to basaltic melts can be expressed as the following Arrhenius relation with compositional dependence, $D_{SiO_2}^{\text{quartz dissolution}} = \exp(-14.168 + 2.758(1 - X) - [(35003 - 38829(1 - X))/T]$, where D_{SiO_2} is in m^2/s and T is in K. The 1σ standard deviation and maximum deviation of the above equation in predicting ln D_{SiO_2} are 0.32 (or 0.14 $\log_{10} D$ units) and 0.95 (or 0.41 $\log_{10} D$ units). Because SiO_2 diffusivity depends on SiO_2 concentration, no theory is currently available to predict diffusive quartz dissolution rate. We develop a method by adopting the formulation for the case of constant D but replacing the constant D by an effective D (D_{eff}), $L = 2\alpha(D_{eff}t)^{1/2}$, where α is solved from the composition of the dissolving crystal, the interface melt and the far-field melt. Using experimental data, the effective diffusivity during mineral dissolution may be related to diffusivity in the farfield ($D_{farfield}$) and interface ($D_{interface}$) melts as follows: $\ln(D_{eff}/D_{farfield}) = (0.6996 + 0.0327Y)Y$, where $Y = \ln(D_{interface}/D_{farfield})$. The method is applied successfully to treat diffusive and convective quartz dissolution rates.

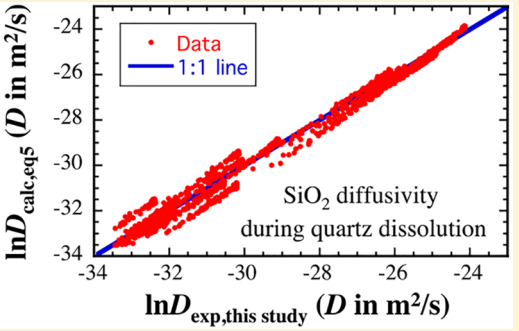

KEYWORDS: *Quartz dissolution kinetics, SiO_2 diffusion, Mineral dissolution rate with variable diffusivity, SiO_2 concentration at quartz saturation, Quartz-melt equilibrium*

1. INTRODUCTION

Quartz is a major mineral in silicic igneous rocks. An understanding of the kinetic interaction between quartz and silicate melts can help model quartz growth and dissolution in melts. In addition, because quartz is a simple stoichiometric mineral, there is no compositional variability for modeling quartz growth and dissolution. Hence, modeling quartz dissolution and growth rates in silicate melts may be more accurate than that of other minerals, and the results may be applied to evaluate magma dynamics and cooling rates.

There have been many studies on different aspects of quartz dissolution in various silicate melts. For example, Watson[1] studied quartz dissolution in a basaltic melt and examined the effect of convection. Zhang et al.[2] conducted an experiment of quartz dissolution in an andesitic melt. Liang[3] investigated the diffusivity matrix during quartz dissolution in a ternary CAS ($CaO–Al_2O_3–SiO_2$) melt system. Shaw[4−7] and Acosta-Vigil[8] focused on the interface reaction between quartz, and natural and various synthetic melts. These studies have provided insight into different aspects of quartz dissolution kinetics. However, there is a need to quantify quartz dissolution and

Received: December 5, 2018
Revised: February 20, 2019
Accepted: February 26, 2019
Published: February 26, 2019

DOI: 10.1021/acsearthspacechem.8b00193
ACS Earth Space Chem. 2019, 3, 599–616

Table 1. Compositions of Quartz and Rhyolitic, Andesitic, and Basaltic Glasses[a,b]

	mineral		rhyolitic glass			andesite	basalt
oxides	quartz	NCO	CIT	KS	H6a	LML[c]	JDF[d]
SiO_2	99.78	72.89	76.3	76.46	74.67	56.5	49.9
SnO_2	nd	nd	nd	nd	nd	nd	nd
TiO_2	0.01	0.22	0.05	0.06	0.26	1.24	1.83
Al_2O_3	0.12	14.23	12.98	12.43	13.44	18.0	13.53
FeO_t	0.11	1.93	0.91	1.02	1.72	6.71	12.93
MnO	0.01	0.06	nd	nd	nd	0.13	0.22
MgO	nd	0.18	0.02	0.03	0.27	3.96	6.81
CaO	0.02	0.86	0.41	0.49	1.22	7.73	10.81
Na_2O	nd	4.73	4.06	4.25	3.92	3.75	2.65
K_2O	0.01	4.24	5.28	5.01	4.49	1.70	0.17
H_2O	nd	0.1	0.1	0.9	5.9	0.02	0.32
dry total	100.06	99.35	100.01	99.75	99.99	99.74	98.85

[a]nd means not determined. [b]SiO_2 to K_2O concentrations in KS and H6a are given on an anhydrous basis for easy comparison. [c]Composition of LML andesite is from Zhang et al. (1989) with H_2O concentration from FTIR measurement. [d]Water content in JDF is given by averaging the range 0.25−0.4 wt % H_2O (Chen and Zhang, 2008)

Table 2. Summary of Experimental Conditions[a,d]

type	exp#	melt used	T (°C)	duration (s)	L_{melt} (μm)	$L_{mineral}$ (μm)
quartz dissolution in rhyolite	QzDisRh103	NCO	1303	172811	12.5	11.6
	QzDisRh111		1304	87060	14.8	13.7
	QzDisRh112		1305	43219	9.0	8.3
	QzDisRh115		1293	346258	24.1	22.3
	QzDisRh201		1294	21583	6.4	5.9
	QzDisRh203		1292	86397	12.9	11.9
	QzDisRh105		1408	86433	36.5	33.8
	QzDisRh113		1414	44970	20.9	19.3
	QzDisRh114		1403	21627	21.2	19.6
	QzDisRh102		1505	14386	17.2	15.9
	QzDisRh104		1501	86432	50.3	46.5
	QzDisRh106		1600	14435	43.8	40.5
quartz dissolution in andesite[b]	234	LML	1300	3600	6.5	6.7
quartz dissolution in basalt	QzDisBa101	JDF	1293	3667	29.6	32.3
	QzDisBa102		1306	918	17.6	19.2
	QzDisBa103		1304	257	8.6	9.4
	QzDisBa110		1394	1232	39.1	42.6
	QzDisBa111		1400	318	17.4	19.0
	QzDisBa104		1508	928	43.3	47.2
	QzDisBa107		1576	322	34.9	38.1
cassiterite dissolution in rhyolite[c]	CassDis8	H6a	950	239	1.5	0.5
	CassDis9		750	634	0.08	0.10
	CassDis6		850	299	0.31	0.09
	CassDis12		850	1519	0.65	0.21
	CassDis10	KS	900	18026	0.67	0.22
	CassDis3		1000	18092	3.4	1.1
	CassDis1		1100	1856	2.6	0.9
	CassDis11	CIT	1000	18000	2.3	0.8
	CassDis13		1100	3633	0.27	0.09

[a]All experiments were conducted at 0.5 GPa pressure condition. Reported experimental temperature T is the corrected temperature using the calibration of ref 38. One micrometer = 10^{-6} m. [b]From ref 2 with L_{melt} and $L_{mineral}$ from our new fit. [c]From ref 17. [d]Melt growth distance L_{melt} is calculated from SiO_2 concentration profiles using mass balance for quartz dissolution and cassiterite dissolution experiments; mineral dissolution distance ($L_{mineral}$) is then calculated by using $L_{mineral} = L_{melt}\rho_{melt}/\rho_{mineral}$, β-quartz density of 2.54 g/cc; NCO, KS, and CIT densities of 2.35 g/cc; H6a density of 2.28 g/cc; LML density of 2.60 g/cc; JDF basalt glass density of 2.77 g/cc; cassiterite density of 6.99 g/cc.

growth rate and SiO_2 diffusivity in different silicate melts. In addition, more data on the interface melt composition during quartz dissolution (i.e., at quartz saturation) can be used to improve thermodynamic models of silicate melts, such as the MELTS software.[9−13] Therefore, a systematic investigation of the kinetics of quartz dissolution in different silicate melts is important to a number of geological problems.

Mineral dissolution may be controlled by either mineral−melt interface reaction or mass transport of the mineral-constituent components in the melts.[2,14] Diffusive mineral

DOI: 10.1021/acsearthspacechem.8b00193
ACS Earth Space Chem. 2019, 3, 599−616

dissolution experiments provide diffusivity data for the equilibrium-determining component, the interface melt composition, and a way to model diffusive and convective dissolution rates as a function of temperature and pressure.[2,15−19] SiO_2 diffusion in silicate melts plays a major role not only in quartz dissolution/growth but also in a wide spectrum of igneous processes, including magma assimilation, double-diffusive convection, and fluid transport of SiO_2. Extensive studies on SiO_2 diffusion, both self-diffusion and effective binary diffusion,[20] have been carried out.[1,2,15−19,21−33] However, prediction of SiO_2 diffusivity as a function of melt composition and temperature is still not available (see review in ref 34).

To quantify the kinetics of quartz dissolution in silicate melts and SiO_2 diffusion during the dissolution process, we have conducted two series of quartz dissolution experiments, one in rhyolitic melt and the other in basaltic melt. The results will be combined with literature data to quantify the saturation conditions of quartz and SiO_2 diffusivity as a function of melt composition during quartz dissolution in rhyolitic, andesitic, and basaltic melts. In addition, quartz dissolution and growth rates in silicate melts will be discussed.

2. SAMPLES, EXPERIMENTS, AND ANALYSES

Gem-quality quartz crystals and natural and synthetic rhyolitic and basaltic glasses were used in the dissolution experiments conducted in a 0.5 in. piston-cylinder apparatus. The quartz crystals are essentially pure SiO_2 (Table 1). For quartz dissolution experiments, two different starting glasses (melts) were used: one is rhyolite from Newberry Crater (NCO in Table 1) and the other is a midocean ridge basalt from Juan de Fuca Ridge (JDF in Table 1). Both are nominally dry. The basalt is a MORB glass sample from the Juan de Fuca Ridge,[35,36] the same as that used in refs 15, 16, and 18 for olivine, diopside, and anorthite dissolution experiments. Literature data on quartz dissolution in an andesitic melt[2] and on cassiterite dissolution in rhyolitic melts[17] will also be used to examine SiO_2 diffusivity in andesitic melt and hydrous rhyolitic melts; their compositions are also listed in Table 1. The rhyolitic glasses of NCO, CIT, KS, and H6a contain 0.1, 0.1, 0.9, and 5.9 wt % H_2O, respectively. NCO, CIT, and KS are natural rhyolites,[37] and H6a is a synthetic rhyolitic glass prepared in the study of Hui et al.[38]

Starting quartz crystals were sectioned into small round disks with top and bottom surfaces perpendicular to its *c*-axis. The disks are ∼1 mm in thickness and 2.4−2.6 mm in diameter. Rhyolitic and basaltic glasses were ground into cylinders about ∼2 mm in length and 2.4−2.6 mm in diameter. The polished faces of a crystal disk and a glass cylinder were stacked together and then packed into a graphite capsule. The polished surfaces at the contact help maintain better contact between glass (to be melted) and quartz crystal when compressed (e.g., minimizing the chance of bubbles at the interface). To ensure gravitational stability in the melt, the quartz disk was placed on top of the glass cylinder. The capsule design is similar to that used in previous plagioclase dissolution experiments.[18] All experiments were run in a piston-cylinder apparatus with 0.5 in. piston using MgO sleeves and $BaCO_3$ cell.

According to the SiO_2 phase diagram (Figure 6 in ref 39), β-quartz is stable between ∼750 and 1700 °C at 0.5 GPa. Hence, our quartz dissolution experiments at 1300−1600 °C and 0.5 GPa were carried out in β-quartz stability field. At all experimental temperature and pressure conditions, the corresponding glass samples were molten. Experimental durations were chosen to be long enough to obtain measurable concentration profiles but short enough to satisfy the semi-infinite boundary condition. Time-series experiments were conducted to rule out convection in the melt and to check the reproducibility of our experiments. A summary of all the experimental conditions is listed in Table 2. During each experimental run, the temperature and pressure were maintained automatically using a programmed temperature controller and a pressure controller. The fluctuation in the experimental temperature maintained by the controller is ±1 °C and that in pressure is ±4 MPa. The experimental procedure has been detailed in ref 18. The temperature gradient is zero at the center of the graphite furnace (roughly the position of the interface) at, about 9 K/mm at 1 mm off the center and 18 K/mm at 2 mm off the center.[38] Reported temperatures and pressures in Table 2 have been corrected using the temperature calibration of ref 38 and pressure calibration of ref 40.

After quench of each experiment, the sample assembly was mounted in epoxy and then ground and polished along the central axis of symmetry until the exposed area of the sample is near maximum. The polished sample was further cleaned using ultrasonic cleaner, dried in a vacuum oven, and then carbon-coated before the electron microprobe analyzer (EMPA) analysis using a Cameca SX100 electron microprobe at the University of Michigan.

The EMPA analysis condition was 15 kV and 5 nA focused beam. Counting times are 60 s for Si, 40 s for Al, 30 s for Fe, Ca, and K, 20 s for Mg and Ti, and 10 s for Mn. Na was counted as one of the first elements on a spectrometer for six 5 s periods, and Na concentration is calculated by extrapolation to zero time. Three to four concentration traverses in the glass next to quartz were measured for each experimental sample from the mineral−glass interface to the far-field melt. The effect of quench cracks in the glass on distances of measured points to interface was corrected by cross-matching different traverses across the cracks. The electron microprobe data of all experimental samples is provided in the Supporting Information.

To augment our data, a quartz dissolution experiment in andesitic melt[2] is reexamined in this study. Furthermore, some cassiterite dissolution experiments in ref 17 also generated significant SiO_2 concentration profiles and are examined in this work for SiO_2 diffusivity. The cassiterite dissolution experiments were carried out in rhyolitic melt containing 0.1−5.9 wt % H_2O and at 750−1100 °C and 0.5 GPa. The goal of their experiments was to investigate tin diffusion and cassiterite dissolution kinetics. The resulting profiles in five experiments (CassDis1, 3, 8, 10, and 11) display significant variations in SiO_2 concentration, providing constraints on the effect of H_2O on SiO_2 diffusion and are used in this study. Table 2 also includes a summary of these experiments.

3. EXPERIMENTAL RESULTS

Run conditions of all experiments are summarized in Table 2. We conducted 12 experiments on quartz dissolution in NCO rhyolitic melt and 7 experiments on quartz dissolution in JDF basaltic melt. Figure 1 shows a back scatter electron (BSE) image of a typical sample with EMPA measurement traverses indicated as red line segments. By comparing all measured traverses within the same experiment, the corresponding

DOI: 10.1021/acsearthspacechem.8b00193
ACS Earth Space Chem. 2019, 3, 599−616

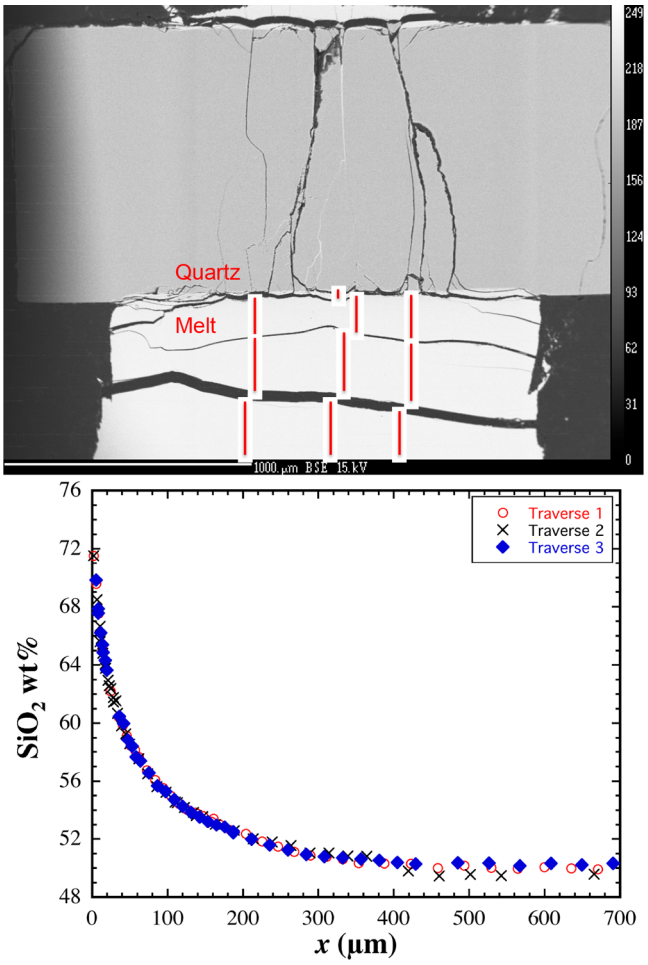

Figure 1. (Top) back-scattered electron image of the experiment sample QzDisBa101 with three measured traverses (red lines) marked on it. (Bottom) SiO_2 concentration profiles for the same sample.

concentration profiles are consistent within error (Figure 1), supporting the absence of convection during the experiments. Consistency among time-series experiments further supports absence of convection.

In quartz dissolution experiments, SiO_2 concentration decreases from the interface melts toward the far-field melts (Figure 1). Figures 2 and 3 show examples of oxide concentration profiles during quartz dissolution in molten rhyolite and basalt, respectively. As quartz dissolves into a silicate melt, the SiO_2 concentration increases toward the quartz–melt interface, and the concentrations of other components (e.g., TiO_2, Al_2O_3, FeO_t, MgO, CaO, Na_2O, and K_2O) are expected to be diluted and to decrease toward the interface. For quartz dissolution into rhyolitic melts (Figure 2), the profiles of these components exhibit the "expected" pattern. During quartz dissolution in basaltic melt (Figure 3), the profiles of SiO_2, TiO_2, Al_2O_3, FeO_t, MgO, and CaO also exhibit the "expected" behavior. However, Na_2O and K_2O profiles show complex uphill diffusion patterns in the basaltic melt toward quartz–melt interface where the SiO_2 concentration is high. The uphill diffusion of Na_2O and K_2O toward the quartz–melt interface is expected to lead to a minimum in the profile (e.g., Figure 9C in ref 41) to satisfy mass balance. However, the minimum is not obvious in Na_2O and K_2O profiles but Na_2O profile shows a maximum. For components with normal diffusion pattern, the concentration profiles usually cannot be fit well by assuming a constant diffusivity (solid red curves in Figures 2 and 3) especially in basaltic melts. Furthermore, the relative lengths of the concentration profiles for the various oxides do not match previously observed differences in the tracer diffusivities:[34] for example, in Figure 2 the K_2O profile is the shortest and Na_2O profile is about the same length as the SiO_2 profile, even though Na and K tracer diffusivities are much higher than SiO_2 diffusivity.[34] These features demonstrate that the diffusion of other components in the systems is largely controlled by SiO_2 diffusion as well as the effects of multicomponent diffusion.[1,33,41] In cassiterite dissolution experiments,[17] SiO_2 concentration decreases toward the cassiterite–melt interface as the dissolution of cassiterite dilutes all major components in the melt.

A summary of interface–melt compositions of all the experiments can be found in Table 3. Figure 4 shows temporal variations of SiO_2 concentration at the interface melt and melt growth distances at different temperature conditions for quartz dissolution. The interface SiO_2 concentrations were obtained by fitting the SiO_2 concentration profiles and extrapolating the profile to the interface. The fitting procedure will be discussed later. For quartz dissolution in rhyolite, the SiO_2 concentration in the interface melt is roughly the same within error at a given experimental temperature (1300, 1400, and 1500 °C) regardless of the experimental duration. For quartz dissolution in basalt experiments, the interface melt concentration of SiO_2 is roughly constant at 1300 °C. There is relatively large variation for the two experiments at 1400 °C (Figure 4b), likely due to both experimental uncertainty (e.g., in the accuracy of the experimental temperature) and uncertainty in extrapolating SiO_2 concentrations to estimate its concentration at the interface melts. Note that the interface melt composition cannot be measured directly even if new instrumentation allows higher spatial resolution because the interface melt were changed were changed by quartz dissolution during quench.[2]

The melt growth distance (L_{melt}) and mineral dissolution distance ($L_{mineral}$) were calculated based on mass balance (eq 16 in ref 2), with $L_{mineral} = L_{melt}(\rho_{melt}/\rho_{mineral})$. Because electron microprobe distances are measured at room temperature and pressure, glass density rather than melt density is used. Because the dissolving mineral during the experiments is β-quartz (not α-quartz), the estimated density of β-quartz, about 2.54 g/cm^3 at room temperature and pressure[39,42] is used. That is, the reported crystal dissolution distance is for β-quartz dissolution. For cassiterite, the density is about 6.99 g/cm^3. Figure 4c,d shows there are good linear relations ($L = b\sqrt{t}$) between the melt growth distance (L) and the square root of the experimental duration ($\sqrt{t}$).

On the basis of both the constancy of the SiO_2 concentration in the interface melt at a given temperature, and the proportionality between the melt growth distance and the square root of the experimental duration, we infer that quartz dissolution in both rhyolitic and basaltic melts is controlled by diffusion of SiO_2, implying rapid interface reaction.

4. DISCUSSION

Diffusion in the melt during quartz dissolution is fundamentally a multicomponent diffusion problem. Major advancement

DOI: 10.1021/acsearthspacechem.8b00193
ACS Earth Space Chem. 2019, 3, 599–616

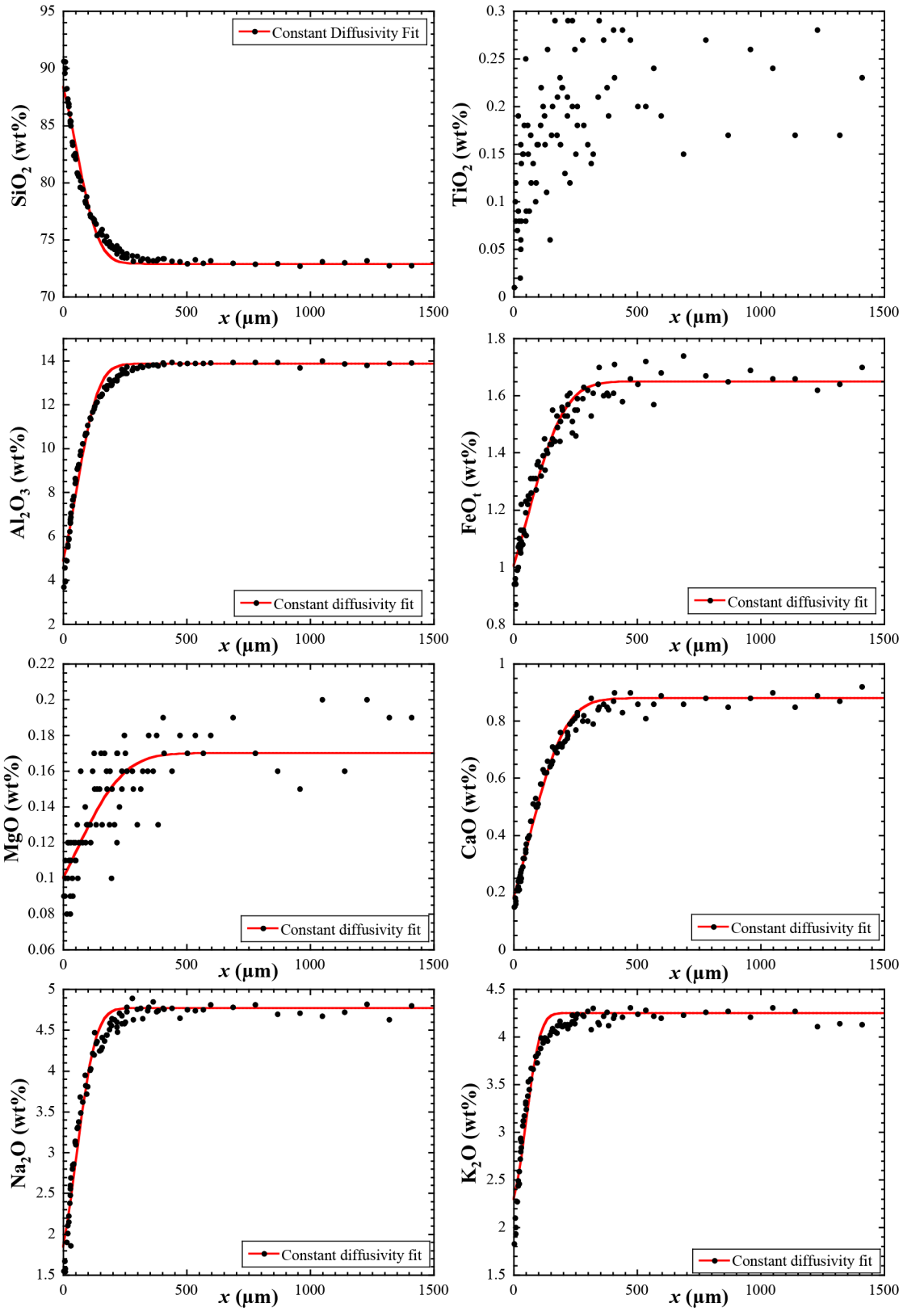

Figure 2. Oxide concentration profiles for a quartz dissolution experiment in a rhyolitic melt (QzDisRh104, 1501 °C, 0.5 GPa, 86432 s).

has been made in treating multicomponent diffusion in natural melts[43−46] but data in this study are not enough to apply a rigorous multicomponent diffusion treatment. One reason is that the experiments in our study do not cover enough compositional directions. For example, refs 45−47 showed that experiments covering at least seven mutually perpendicular compositional directions (preferably more experiments) are needed for an eight-component melt system. Second, as it

DOI: 10.1021/acsearthspacechem.8b00193
ACS Earth Space Chem. 2019, 3, 599−616

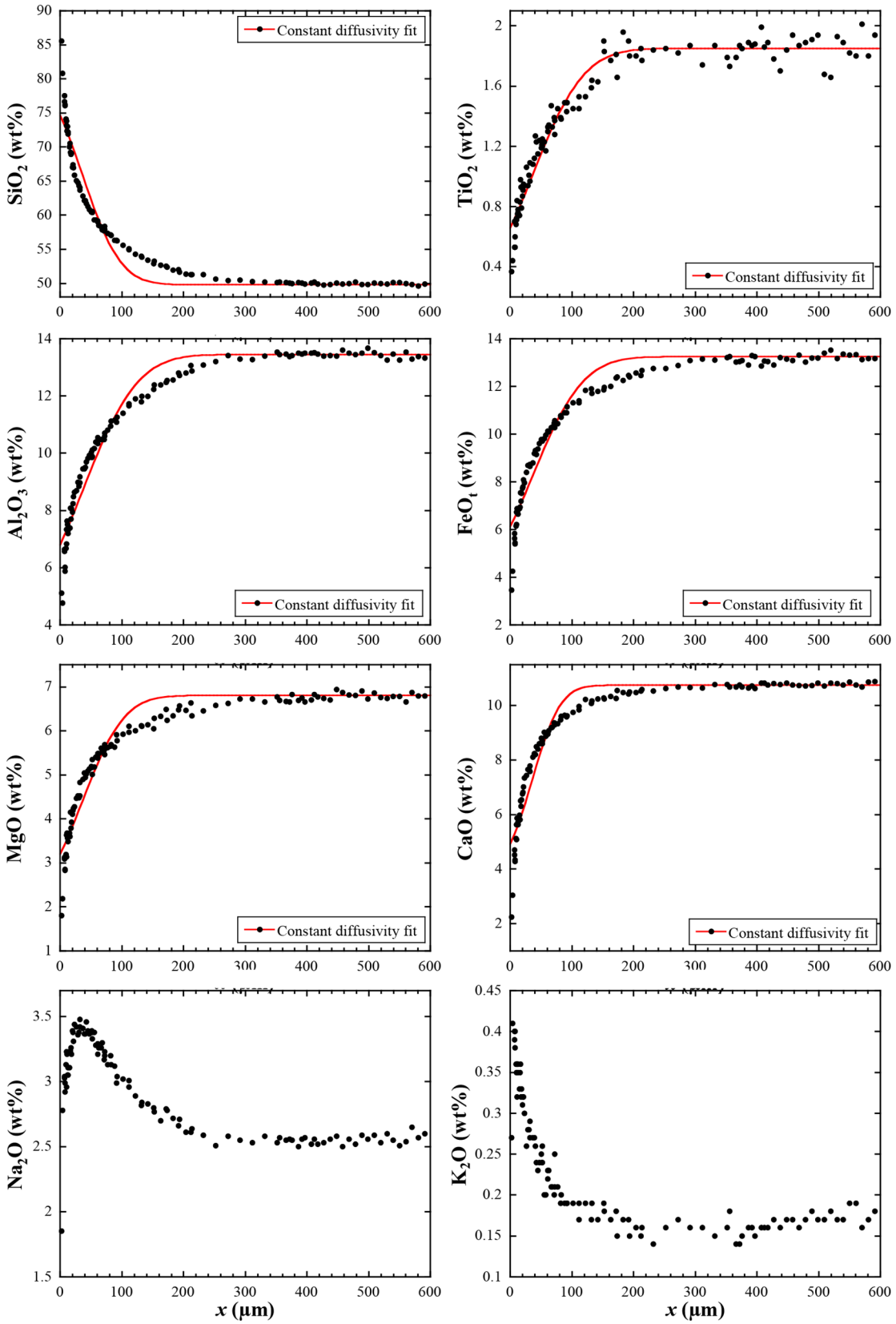

Figure 3. Oxide concentration profiles for a quartz dissolution experiment in a basaltic melt (QzDisBa107, 1576 °C, 0.5 GPa, 322 s).

will be clear soon, the diffusion coefficients in the melt vary across a diffusion profile during quartz dissolution due to large variation in SiO_2 concentration, meaning that the diffusion matrix is not a constant matrix, further complicating the multicomponent diffusion treatment.

DOI: 10.1021/acsearthspacechem.8b00193
ACS Earth Space Chem. 2019, 3, 599−616

Table 3. Extrapolated Interface−Melt Compositions of All Experiments[a,b]

sample#	SiO_2	SnO_t	TiO_2	Al_2O_3	FeO_t	MnO	MgO	CaO	Na_2O	K_2O	total
QzDisRh103	82.96		0.13	8.8	1.3	0.03	0.07	0.28	3.5	3.1	100.17
QzDisRh111	85.61		0.10	6.4	1.1	0.04	0.09	0.21	3.0	2.9	99.45
QzDisRh112	84.22		0.12	7.8	1.2	0.05	0.09	0.28	2.6	2.9	99.26
QzDisRh115	83.86		0.13	7.8	1.3	0.02	0.10	0.30	3.1	3.0	99.61
QzDisRh201	84.92		0.10	7.5	1.5	0.05	0.11	0.30	2.2	3.2	99.88
QzDisRh203	84.58		0.13	7.3	1.3	0.04	0.12	0.26	2.3	3.0	99.03
QzDisRh105	90.14		0.10	3.9	0.9	0.02	0.07	0.14	1.3	1.8	98.37
QzDisRh113	88.02		0.14	5.8	1.2	0.05	0.09	0.20	2.3	2.4	100.20
QzDisRh114	89.26		0.05	4.6	1.1	0.05	0.08	0.18	1.5	2.0	98.82
QzDisRh102	90.92		0.15	4.8	1.1	0.04	0.07	0.14	1.8	2.3	101.32
QzDisRh104	91.40		0.06	3.4	0.9		0.08	0.13	1.4	1.7	99.07
QzDisRh106	95.38		0.06	0.9	0.8		0.06	0.08	0.8	0.8	98.88
Andesite-234	82.55		0.44	8.0	2.0	0.05	1.0	1.7	1.9	2.45	100.09
QzDisBa101	73.54		0.82	8.1	6.1	0.09	3.10	5.00	3.6	0.5	100.81
QzDisBa102	71.52		0.78	8.1	6.3	0.09	3.15	4.90	4.0	0.5	99.29
QzDisBa103	71.87		0.73	8.5	6.6	0.10	3.30	5.50	3.7	0.4	100.70
QzDisBa110	80.29		0.55	5.9	4.0	0.03	2.20	3.20	2.9	0.5	99.52
QzDisBa111	75.99		0.72	7.1	5.6	0.06	2.80	4.20	3.1	0.5	100.02
QzDisBa104	90.02		0.26	5.1	2.2		0.50	0.00	0.9	0.5	99.48
QzDisBa107	92.66		0.32	3.5	1.4		0.50	0.00	1.1	0.5	99.98
CassDis8	66.39	5.00	0.25	12.2	2.0		0.28	1.57	3.4	3.8	94.89
CassDis10	70.71	5.37	0.06	11.1	1.3		0.03	1.30	3.7	4.2	97.77
CassDis3	68.62	9.56	0.06	11.2	1.3		0.03	1.00	3.3	4.0	99.07
CassDis1	64.15	12.83	0.06	10.8	1.4		0.03	1.10	3.3	3.8	97.47
CassDis11	66.00	12.49	0.05	10.3	1.3		0.02	1.20	3.5	3.5	98.36

[a] FeO_t stands for total iron oxide expressed as FeO, and similar for SnO_t. Interface−melt concentrations were estimated by visual fits of the concentration profiles to the interface except for SiO_2 whose values were from fitting SiO_2 concentration profiles using eq 4, and for SnO_t for cassiterite dissolution experiments. [b] Cassiterite dissolution experiments with no discernible or low-quality SiO_2 concentration profiles are not included.

The main purpose of this work is to understand the kinetics of quartz dissolution and quantify diffusive dissolution rates, which are largely controlled by SiO_2 diffusion. The concentration profiles of SiO_2 in the melt during quartz dissolution are smooth and monotonic, which lend themselves to the effective binary diffusion approach.[20] This is consistent with the conclusion of ref 2 that the diffusion of the principal equilibrium-determining component (SiO_2 in the case of quartz dissolution) can be roughly treated as effective binary. The diffusion of other components is of interest but less important for understanding quartz dissolution kinetics, and hence is not treated in this work. Nonetheless, the complete electron microprobe data of all oxides are provided in Supporting Information, which may be used for multicomponent diffusion treatment when more data are available or for other purposes. Below, we will first discuss the fitting of SiO_2 concentration profiles during quartz dissolution to obtain the effective binary diffusivity (EBD) of SiO_2. We show that EBD of SiO_2 depends strongly on melt composition, in agreement with previous authors.[1,21,23,28,33] We fit SiO_2 concentration profile during quartz dissolution and make an effort to quantify how SiO_2 diffusivity depends on melt composition. The fitting of SiO_2 diffusion profile also provides the SiO_2 concentration at the quartz−melt interface, which approximates the SiO_2 concentration at quartz saturation (SCQS). The variation of SCQS will be examined, and the results will be useful for constraining thermodynamic models for silicate melts (such as the MELTS model[9−13]). We then develop a method to quantify quartz dissolution rate considering composition-dependent SiO_2 diffusivity, which has general applicability to dissolution or growth of other minerals when the EBD of the equilibrium-determining component varies along the diffusion profile (e.g., cassiterite dissolution[17]).

4.1. Fitting SiO_2 Concentration Profiles from Quartz Dissolution Experiments. For diffusion-controlled mineral dissolution, if the effective binary diffusivity of a given component is constant across the whole concentration profile, the concentration profile can be fit by the following equation[2]

$$C = C_\infty + (C_0 - C_\infty)\frac{\mathrm{erfc}\left(\frac{x}{\sqrt{4Dt}} - \alpha\right)}{\mathrm{erfc}(-\alpha)} \quad (1)$$

in which α is solved from the following

$$\sqrt{\pi}\alpha e^{\alpha^2}\mathrm{erfc}(-\alpha) = \frac{C_0 - C_\infty}{C_c - C_0} \quad (2)$$

where C_∞, C_0, C_c, and C are the concentrations of the diffusing component in the far-field melt, interface melt, the crystal, and the melt at distance x away from the mineral−melt interface, D is the EBD of the diffusing component, and t is the experimental duration.

However, a comparison (Figures 2, 3, and 5) between the SiO_2 concentration data and the constant-diffusivity model (eq 1) shows obvious misfit (more so for quartz dissolution in basalt), indicating that there is significant variation in the SiO_2 EBD across the concentration profile. Furthermore, the misfit is systematic with data forming steeper trend at higher SiO_2 and shallower trend at lower SiO_2 compared to the constant-diffusivity curve. This indicates that D decreases with

DOI: 10.1021/acsearthspacechem.8b00193
ACS Earth Space Chem. 2019, 3, 599−616

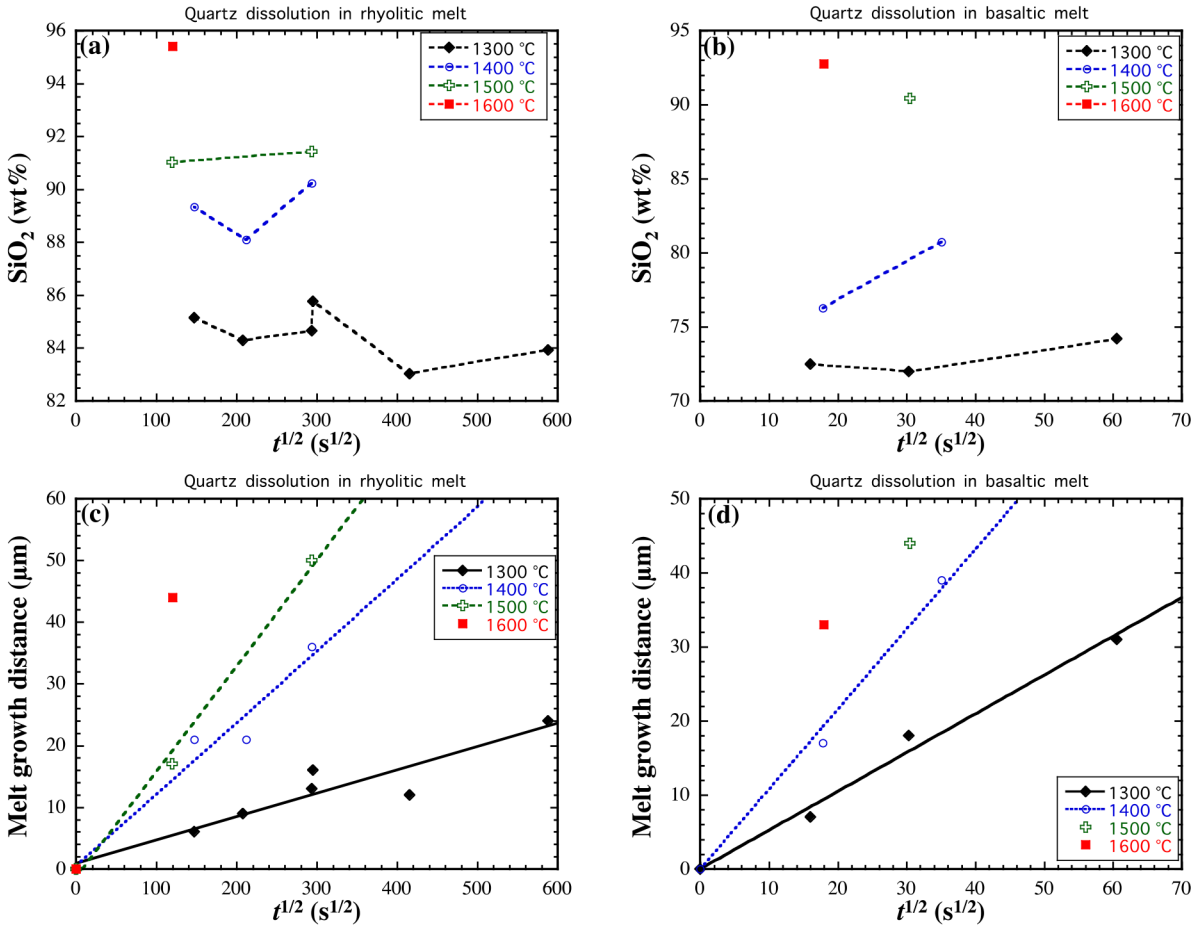

Figure 4. (a,b) SiO_2 concentrations in the melt at quartz−melt interface versus the experimental duration for quartz dissolution experiments in rhyolite and basalt respectively. (c,d) Variation of melt growth distance with time for the two sets of quartz dissolution experiments. Melt growth distances were calculated using mass balance.

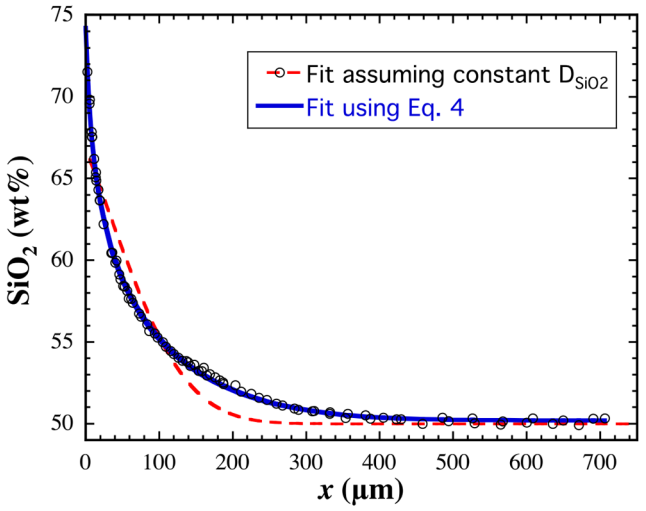

Figure 5. Typical SiO_2 concentration profile (black open circles, sample QzDisBa101) and fitting results using constant diffusivity of eq 1 (red dash curve) and composition-dependent diffusivity of eq 4 (blue solid curve).

increasing SiO_2, as previously demonstrated.[1,21,23,28,33] Therefore, it is necessary to quantify how the EBD of SiO_2 varies along a profile. Below, we will use both the Boltzmann analysis and the fit of concentration profiles using a functional dependence of $D(C)$ to determine the compositional dependence of SiO_2 EBD.

4.1.1. Boltzmann Analysis of Concentration Profiles from Quartz Dissolution Experiments. In diffusion-couple experiments, Boltzmann−Matano analysis[48] or the Sauer-Freise analysis[49] has been applied to investigate the compositional dependence of diffusivity.[1,21,23,28,33,50] The quality of such an approach largely depends on the precision of the original data of the concentration profiles. It has been shown[1,21,23,28,33] that ln D_{SiO_2} depends roughly linearly on the SiO_2 concentration. Below, we use a similar Boltzmann approach, and derive the following equation (Appendix A) to calculate the diffusivity at each point (also meaning each concentration) using concentration profiles generated by mineral dissolution experiments

$$D = \frac{\frac{C_\infty - C_x}{C_c - C_\infty}\int_{C_0}^{C_\infty} x\,\mathrm{d}C + \int_{C_x}^{C_\infty} x\,\mathrm{d}C}{2t\frac{\partial C}{\partial x}\Big|_x}, \quad t > 0 \tag{3}$$

where C_x is SiO_2 concentrations in the melt at distance x away from the mineral−melt interface. Note here that the interface position is known and fixed for the case of mineral dissolution experiments, rather than the adjustable Matano interface[48] for the case of diffusion couple. In addition, diffusion must not

DOI: 10.1021/acsearthspacechem.8b00193
ACS Earth Space Chem. 2019, 3, 599−616

Table 4. Summary of Fitting Results for Quartz Dissolution Experiments Based on Equation 4[a]

exp#	β	B (10^{-6} m/s$^{1/2}$)	C_0 (wt %)	ln $D_{X=1}$ (m^2/s)	ln $D_{farfield}$ (m^2/s)	ln $D_{interface}$ (m^2/s)	ln D_{eff} (m^2/s)
QzDisRh103	23.92(19)	0.0155(3)	82.96(19)	−36.60(23)	−32.42(21)	−33.60	−33.19
QzDisRh111	23.92(19)	0.0235(4)	85.61(20)	−36.04(23)	−31.92(21)	−33.50	−32.89
QzDisRh112	23.92(19)	0.0216(3)	84.22(11)	−35.69(23)	−31.95(21)	−33.25	−32.78
QzDisRh115	23.92(19)	0.0211(3)	83.86(10)	−36.12(23)	−31.81(21)	−33.34	−32.76
QzDisRh201	23.92(19)	0.0221(4)	84.92(32)	−35.76(23)	−32.03(21)	−33.45	−32.90
QzDisRh203	23.92(19)	0.0209(2)	84.58(10)	−35.96(23)	−31.98(21)	−33.53	−32.93
QzDisRh105	22.75(15)	0.0595(5)	90.14(9)	−34.28(19)	−30.56(17)	−32.71	−31.89
QzDisRh113	22.75(15)	0.0464(8)	88.02(19)	−34.85(19)	−30.82(17)	−32.70	−32.00
QzDisRh114	22.75(15)	0.0695(7)	89.26(14)	−33.88(19)	−30.22(17)	−32.17	−31.44
QzDisRh102	21.55(12)	0.0717(9)	90.92(31)	−34.02(15)	−30.18(14)	−32.59	−31.65
QzDisRh104	21.55(12)	0.0809(8)	91.40(11)	−33.70(16)	−30.10(14)	−32.34	−31.49
QzDisRh106	19.53(14)	0.1723(13)	95.83(17)	−32.38(17)	−29.13(16)	−31.64	−30.73
QzDisBa101	23.92(19)	0.2376(28)	73.54(23)	−35.52(21)	−26.28(16)	−30.12	−28.28
QzDisBa102	23.92(19)	0.2794(23)	71.52(23)	−35.11(21)	−25.87(16)	−29.45	−27.75
QzDisBa103	23.92(19)	0.2729(25)	71.87(25)	−35.21(21)	−25.98(16)	−29.36	−27.82
QzDisBa110	22.75(15)	0.4992(51)	80.29(27)	−33.73(17)	−24.96(13)	−30.01	−27.51
QzDisBa111	22.75(15)	0.4729(47)	75.99(22)	−33.79(17)	−24.99(13)	−29.15	−27.18
QzDisBa104	21.55(12)	0.7018(54)	90.02(42)	−32.72(14)	−24.45(11)	−30.92	−27.77
QzDisBa107	19.53(14)	0.9570(82)	92.66(48)	−31.72(16)	−24.17(13)	−30.31	−27.44

[a]The values in the parentheses indicate 1σ errors on the last digit based on the fitting, but the true error is best gauged from experiments at the same temperature (same β value).

have reached the far-field so that the diffusion medium is semi-infinite.

To implement the above approach, a MatLab program was written in which a profile is first smoothed using a moving average filter with a span of 10 points or more. The integral and slope in eq 3 are calculated using the smoothed profile. Then D at a given position (or given concentration) is calculated using eq 3. Near the far-field, concentration slopes in the denominator of eq 3 approach zero and cannot be evaluated accurately. Near the interface, the concentration profile is steep and the slopes are not well constrained. Hence, the calculated D values at both ends of the concentration profile are usually less accurate and show large fluctuations. To examine the compositional dependence of D, we plot ln D versus SiO_2 concentration as in previous studies.[1,21,23,28,33] Only the smooth part of the trend in the middle concentration range (e.g., for exp. QzDisBa110, C_∞= 50.0 wt %, C_0= 80.3 wt %, but only D values from 52 to 74 wt % SiO_2) is chosen. The results are plotted in Figure 6.

We first examine how ln D_{SiO_2} depends on SiO_2 concentration (left-hand side in Figure 6). We note that ln D_{SiO_2} is roughly linear to SiO_2 concentration (meaning that D_{SiO_2} is roughly an exponential function of SiO_2 concentration) in a given starting melt and at a given temperature, consistent with previous results.[1,21,23,28,33] However, there is a significant offset among the trends (i.e., different intercepts) at the same temperature when comparing the trends across different initial melts (rhyolite, andesite, and basalt) with SiO_2 content as the compositional parameter, indicating that other compositional parameters also influence SiO_2 diffusion.

We next examine ln D versus X_{Si+Al} plot (right-hand side of Figure 6), where X_{Si+Al} is the sum of cation mole fractions of Si and Al (for the benefit of readers, the Supporting Information contains examples for the calculation of X_{Si+Al} for basalt far-field composition). The data show that using X_{Si+Al} as the compositional parameter reduces the disparity among the different melts. A single trend approximately captures the SiO_2 diffusion behavior across rhyolitic, andesitic, and basaltic melts considering uncertainties as gauged by multiple experiments of quartz dissolution in rhyolitic melts. These observations indicate that X_{Si+Al} (simplified as X hereafter) is a better parameter to characterize the compositional effect on SiO_2 EBD than using SiO_2 alone. That D_{SiO_2} depends on the cation mole fraction of both Si and Al is not surprising because both Si and Al are network formers controlling melt structure and viscosity. In plagioclase dissolution experiments, ref 18 reached a similar conclusion that Si and Al together control the diffusivities of Al_2O_3. Reference 19 also showed that Zr diffusivity depends on Si+Al rather than on SiO_2 alone. Nonetheless, there are still minor offsets in the ln D_{SiO_2} versus X linear trends for different melts; the maximum offset is about 1.1 ln D units at 1500 °C. The offsets are largely within data uncertainty, but they may also be due to the effect of other compositional parameters (e.g., alkali earth elements and alkali elements) on D_{SiO_2}, which cannot be resolved currently.

4.1.2. Fitting SiO_2 Profiles by Using Exponential Dependence of SiO_2 Diffusivity. The major advantage of using Boltzmann analysis to extract diffusivity as a function of composition is that no prescribed functional dependence is assumed and hence the relation is unbiased. However, this method is sensitive to the smoothness of a concentration profile. In addition, there is some arbitrariness in choosing which part of the $D(C)$ relation is the reliable part. To further verify and quantify the relation between SiO_2 EBD and melt composition, we fit the SiO_2 concentration profiles assuming D depends on C or X exponentially based on insights from the preceding section and from the literature.[1,21−28,33,34,50−52] The following diffusivity relation is adopted

$$D = D_{interface} e^{-\beta,(C-C_0)} = D_{farfield} e^{-\beta,(C-C_\infty)} = D_{C=100} e^{\beta,(100-C)} \quad (4a)$$

$$D = D_{interface} e^{-\beta(X-X_0)} = D_{farfield} e^{-\beta(X-X_\infty)} = D_{X=1} e^{\beta(1-X)} \quad (4b)$$

DOI: 10.1021/acsearthspacechem.8b00193
ACS Earth Space Chem. 2019, 3, 599−616

Table 5. Summary of ln D_{SiO_2} from Fitting Results Based on Equation 4

			ln D (m^2/s)						
exp#	β	ln $D_{X=1}$ (m^2/s)	X = 0.65	X = 0.70	X = 0.75	X = 0.80	X = 0.85	X = 0.90	X = 0.95
QzDisRh103	23.92(19)	−36.60(23)	−28.23	−29.43	−30.62	−31.82	−33.01	−34.21	−35.41
QzDisRh111	23.92(19)	−36.04(23)	−27.67	−28.87	−30.07	−31.26	−32.46	−33.65	−34.85
QzDisRh112	23.92(19)	−35.69(23)	−27.32	−28.52	−29.71	−30.91	−32.10	−33.30	−34.50
QzDisRh115	23.92(19)	−36.12(23)	−27.75	−28.94	−30.14	−31.34	−32.53	−33.73	−34.92
QzDisRh201	23.92(19)	−35.76(23)	−27.39	−28.59	−29.78	−30.98	−32.17	−33.37	−34.57
QzDisRh203	23.92(19)	−35.96(23)	−27.59	−28.79	−29.98	−31.18	−32.37	−33.57	−34.77
QzDisRh105	22.75(15)	−34.28(19)	−26.31	−27.45	−28.59	−29.73	−30.86	−32.00	−33.14
QzDisRh113	22.75(15)	−34.85(19)	−26.89	−28.03	−29.17	−30.30	−31.44	−32.58	−33.72
QzDisRh114	22.75(15)	−33.88(19)	−25.92	−27.06	−28.19	−29.33	−30.47	−31.61	−32.74
QzDisRh102	21.55(12)	−34.02(15)	−26.48	−27.56	−28.63	−29.71	−30.79	−31.87	−32.94
QzDisRh104	21.55(12)	−33.70(16)	−26.16	−27.23	−28.31	−29.39	−30.47	−31.54	−32.62
QzDisRh106	19.53(14)	−32.38(17)	−25.54	−26.52	−27.50	−28.47	−29.45	−30.43	−31.40
QzDisBa101	23.92(19)	−35.52(21)	−27.15	−28.35	−29.54	−30.74	−31.94	−33.13	−34.33
QzDisBa102	23.92(19)	−35.11(21)	−26.74	−27.94	−29.13	−30.33	−31.53	−32.72	−33.92
QzDisBa103	23.92(19)	−35.21(21)	−26.84	−28.03	−29.23	−30.42	−31.62	−32.81	−34.01
QzDisBa110	22.75(15)	−33.73(17)	−25.77	−26.91	−28.05	−29.18	−30.32	−31.46	−32.60
QzDisBa111	22.75(15)	−33.79(17)	−25.83	−26.96	−28.10	−29.24	−30.38	−31.51	−32.65
QzDisBa104	21.55(12)	−32.72(14)	−25.18	−26.25	−27.33	−28.41	−29.49	−30.56	−31.64
QzDisBa107	19.53(14)	−31.72(16)	−24.89	−25.86	−26.84	−27.82	−28.79	−29.77	−30.75

[a] SiO_2 diffusivities at specific melt compositions (X_{Si+Al}= 0.65, 0.7, 0.75, 0.8, 0.85, 0.9, 0.95) are calculated based on eq 4. The values in the parentheses indicate 1σ errors on the last digit based on the fitting.

where C is SiO_2 wt %, $X = X_{Si+Al}$, D, $D_{interface}$, $D_{farfield}$, $D_{C\ =\ 100}$, and $D_{X=1}$ are the SiO_2 diffusivity in the melt of composition C, interface melt (C_0), the far-field melt (C_∞), 100% SiO_2, and when X = 1; β' and β characterize the dependence of the diffusivity on SiO_2 (wt %) and X. Our approach here is similar to that in refs 17 and 33, though in ref 17 Sn and Si diffusivities near the interface are higher than that in the far-field melt, whereas during quartz dissolution Si diffusivity near the interface is lower than that in the far-field melt.

In the model, the melt growth rate is $V_{melt} = B/\sqrt{t}$, where B is an unknown constant to be obtained from fitting (related to mass balance). We numerically solve the diffusion−dissolution equation in semi-infinite space (eqs (A1) and (A2) in Appendix A) with concentration-dependent D given in eq 4. A nonlinear least-squares method based on Levenberg−Marquardt algorithm is used to minimize the sum of squares of errors along a concentration profile. The fitting yields values of $D_{X=1}$ and β from which EBD of SiO_2 at various points including $D_{farfield}$ and $D_{interface}$ can be calculated. It turns out that the SiO_2 profile in each individual experiment does not necessarily constrain the parameters well due to correlated errors in β and $D_{X=1}$, though the profiles in basaltic melts provide better constraints owing to a larger compositional span. To improve the fitting, we fit all the concentration profiles (regardless of initial melt compositions and experimental durations) at the same experimental temperature (e.g., ~1300 °C) together to obtain a single β value while allowing $D_{X=1}$ to vary from one experiment to another, because the slopes in the plot of ln D versus either SiO_2 or X are almost the same at the same experimental temperature in rhyolite and basalt (Figure 6). The benefit of doing so is to best constrain the parameters of β. All fitting results are summarized in Table 4. SiO_2 diffusivities at intermediate melt compositions (X_{Si+Al}= 0.65, 0.7, 0.75, 0.8, 0.85, 0.9, and 0.95) are provided in Table 5. In addition, SiO_2 diffusivities along the melt composition profiles are provided in Supporting Information. A comparison between the fit concentration profile and the measured data is illustrated in Figure 5 as the blue solid curve. Other fits are shown in Supporting Information. The D versus C relations obtained from the fits are shown in Figure 6 as lines (red dash lines for quartz dissolution in basalt, and blue dash lines for quartz dissolution in rhyolite), which are in good agreement with the numerical results using the Boltzmann analysis (Figure 6).

4.1.3. Compositional and Temperature Dependence of SiO_2 Diffusivity in Silicate Melts. In this study, the time-series experimental design and the wide range of experimental temperatures and melt composition enable us to assess the compositional dependence of D_{SiO_2} on both Si and Al, and to evaluate how it relates to the temperature. Fitting D_{SiO_2} values in Supporting Information Tables 1 and 2 (2046 points) as a function of X and T (X > 0.6; T = 1300−1600 °C) leads to

$$D_{SiO_2}^{\text{quartz dissolution}} = \exp\left(-14.168 + 2.758(1 - X) - \frac{35003 - 38829(1 - X)}{T}\right) \quad (5)$$

where X is the cation mole fraction of Si + Al and T is in K. The above equation reproduces our data (Supporting Information Tables S1 and S2) with 1σ standard deviation of 0.32 ln D units and maximum deviation of 0.95 ln D units. Extrapolation for applications to 800 to 1200 °C will introduce additional errors. In calculating X, H in H_2O (e.g., 0.32 wt % H_2O in JDF) is included in the cations. Although eq 5 is applicable to rhyolitic to basaltic melts, calculation of X requires the full melt composition, which is sometimes unavailable or inconvenient. Hence, we also relate D_{SiO_2} for quartz dissolution in individual melts to SiO_2 wt % (C) and T as follows

DOI: 10.1021/acsearthspacechem.8b00193
ACS Earth Space Chem. 2019, 3, 599−616

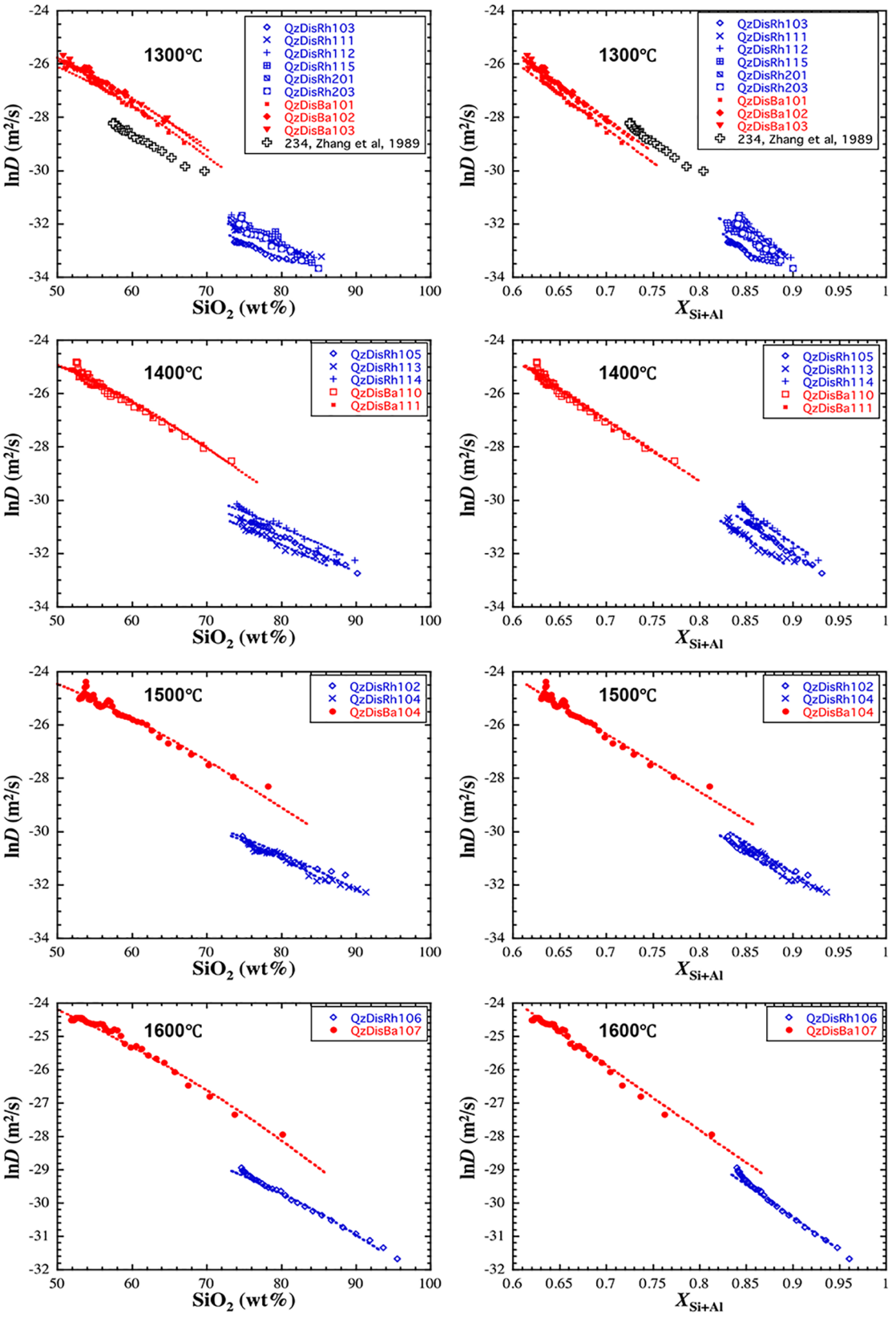

Figure 6. SiO_2 diffusivity from Boltzmann analyses (points) and functional fitting results (dash line) as a function of SiO_2 concentration (left column) and X (right column). The analyzed samples are quartz dissolution experiments in rhyolitic (Newberry) and basaltic (JDF) melts at 1300, 1400, 1500, and 1600 °C. One quartz dissolution experiment in andesitic melt at 1300 °C is from ref 2.

DOI: 10.1021/acsearthspacechem.8b00193
ACS Earth Space Chem. 2019, 3, 599−616

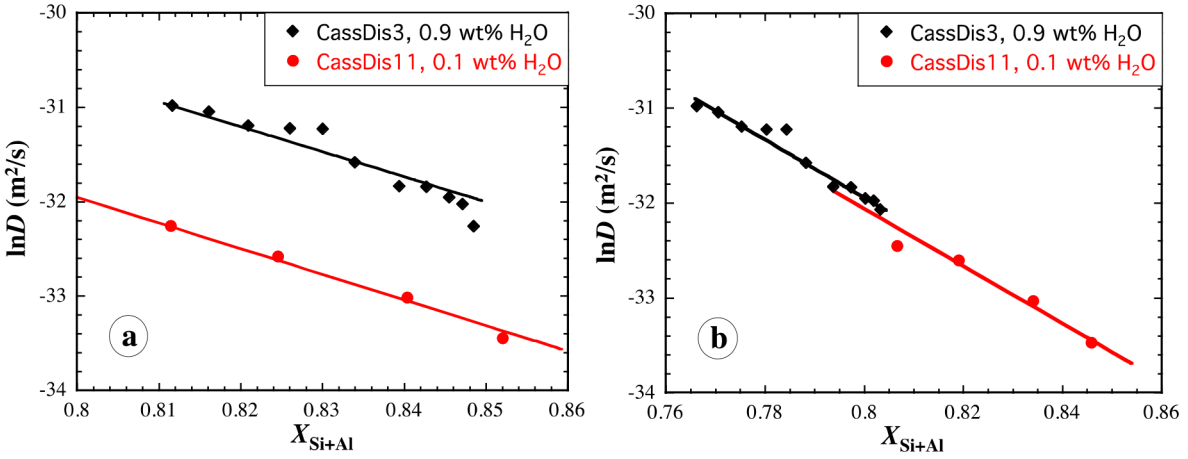

Figure 7. Data points from Boltzmann analyses and functional fitting results (solid lines) of two cassiterite dissolution experiments in CIT and KS rhyolitic melts at 1000 °C. (a) Si and Al cation mole fractions are calculated based on the dry composition; that is, H_2O was ignored when calculating X; (b) H_2O was included by considering H as a cation when calculating X.

$$D_{SiO_2}^{\text{qz diss in rhyolite}} = \exp\left(-7.086 - 0.09469C - \frac{26109 + 28.77C}{T}\right) \quad (6a)$$

$$D_{SiO_2}^{\text{qz diss in basalt}} = \exp\left(-14.751 + 0.02051C - \frac{5052 + 280.5C}{T}\right) \quad (6b)$$

The maximum error in reproducing experimental data is 0.6 to 0.7 ln D units for both. That is, the equations for specific melt systems are more accurate than eq 5.

4.1.4. Effect of H_2O on SiO_2 Diffusivity. Volatiles, especially H_2O, have long been demonstrated to have significant and complex effects on diffusivities of other components.[23−26,34,50,53] The addition of H_2O in silicate melts usually accelerates significantly the diffusion of other components. Such phenomena have often been attributed to the depolymerization of the melt structure by H_2O. Quantitative attempts to model these effects have often treated H_2O concentration as a separate parameter assuming various relations (such as linear, logarithmic, and square root) between D and H_2O content.[34]

We used cassiterite dissolution experiments in various hydrous rhyolitic melts[17] to examine the effect of H_2O on SiO_2 diffusivity. Two of the experiments (CassDis3 and CassDis11) were conducted at the same experimental temperature (1000 °C) in rhyolites with 0.9 wt % H_2O and 0.1 wt % H_2O. ln D versus X data are shown in Figure 7. When X is calculated based on dry glass composition, the ln D versus X trends of these two experiments clearly offset by about 1.4 ln D units (Figure 7a). However, when including H the same way as other cations (such as Fe, Ca, Na) in the calculation of X, the ln D versus X plots of the two experiments fall into the same trend within errors (Figure 7b). Hence, the effect of H_2O on Si diffusivity appears to be the simple dilution of the mole fraction of network forming cations (Si and Al). The experiments at 5.9 wt % H_2O would provide much better constraints but these experiments were at lower temperatures and only one experiment has barely resolvable SiO_2 concentration gradients, unable to provide strong constraints. Nonetheless, Zr diffusivity is also consistent with this observation to higher H_2O contents.[19]

4.1.5. Comparison with Literature Data. Many authors investigated SiO_2 diffusion in silicate melts.[1,21−26,31−34,50] Here, we test our model (eq 5) using literature data. Note that our study reports effective binary diffusivities of SiO_2. Because SiO_2 effective binary diffusivities can depend on concentration gradients even in the same bulk composition,[20,45,46] Equation 5 is best applied to SiO_2 diffusion during quartz dissolution. However, there are no literature data on SiO_2 diffusivities during quartz dissolution for direct comparison (e.g., ref 1 conducted quartz dissolution experiments but did not report SiO_2 diffusivities for these experiments; diffusion data during quartz dissolution in ref 2 are used in this study). Hence, we will use all Si diffusion data on silicate melts with composition close to natural melts for tests. Self-and chemical diffusion data for Si are reviewed in ref 34; data in the review are used but those on albite melt, diopside melt, CAS melt, and $Na_2Si_4O_9$ melt are excluded (the compositions of these melts are far from natural silicate melts). Data with 13 wt % H_2O in ref 23 are excluded because the prediction is far off and because of uncertainty in the H_2O concentration. The H_2O content in the used data in Figure 8 ranges from 0 to 6.7 wt %. Additionally, recent SiO_2 effective binary diffusion data[45,46,50] are also included. Because eq 5 does not evaluate the pressure effect, data with $P > 2$ GPa are excluded. The comparison is shown in Figure 8. Equation 5 predicts Si self-diffusivities[31,32,54] to 0.11 ± 0.55 ln$D$ units, the effective binary diffusivities during dissolution of olivine, diopside, rutile, spinel, and anorthite[2,15,16,55,56] to −0.02 ± 0.73 ln D units, the effective binary diffusion data of Gonzalez−Garcia et al.[50] from diffusion couple experiments to −0.97 ± 0.59 ln D units, the tracer and effective binary diffusivities of Baker and co-workers[22,24−26,57,58] to −0.90 ± 1.27 ln D units, and the effective binary diffusivities of other authors[23,27,45,46,59,60] to −0.34 ± 0.93 ln D units. Notably, Si effective binary diffusivities during mineral dissolution and self-diffusivities are well predicted. The largest discrepancy is for the diffusion data by Baker and co-workers. Some of the discrepancies may be attributed to (i) the effect of the halogens in their experiments, (ii) the use of one single parameter X (= Si + Al) to capture the compositional effect (including the effect of H_2O) of complicated silicate melts, and (iii) the variable concentration gradients, leading to additional deviations.[45,46]

4.1.6. Relation between SiO_2 Diffusivity and Melt Viscosity. There is much expectation that SiO_2 diffusivity is related to melt viscosity. For example, SiO_2 tracer diffusivity might be the same as Eyring diffusivity.[34,61] Mungall[62]

DOI: 10.1021/acsearthspacechem.8b00193
ACS Earth Space Chem. 2019, 3, 599−616

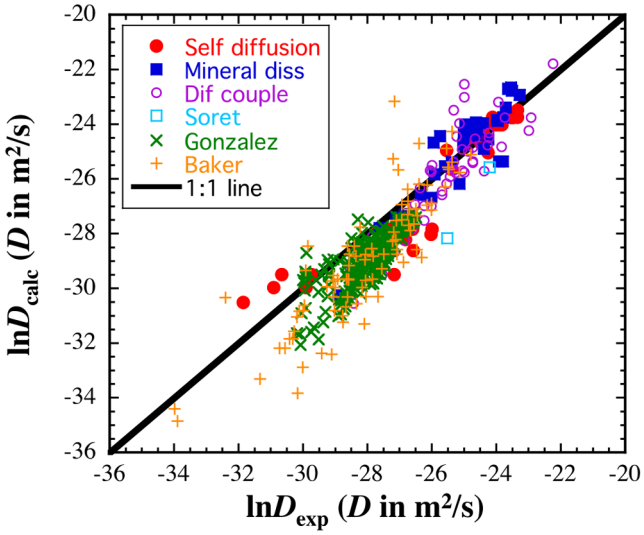

Figure 8. Testing eq 5 using literature SiO_2 diffusion data. Data coverage: temperature between 900 and 1710 °C, pressure ≤ 2 GPa, H_2O ≤ 6.7 wt %. Soret diffusion data are from ref 21. Gonzalez mean are from ref 50, whose data are plotted separately partially because the data set contained 242 points, more than all other data combined. Sources of other data can be found in the text.

proposed a relation between the tracer diffusivity of high-field strength elements and viscosity. Note that SiO_2 diffusivities obtained in this study are effective binary diffusivities, rather than tracer diffusivities. Figure 9 compares experimental SiO_2 EBD from this work to Eyring diffusivities and those by the model of Mungall.[62] In calculating the Eyring diffusivities, the viscosity models of refs 63 and 64 are used, and the jumping distance is assumed to be 0.28 nm. The choice of 0.28 nm is because Si tracer diffusivity in dry melts is often similar to oxygen tracer diffusivity[34] and 0.28 nm is the diameter of the O^{2-} ion. The comparisons show that either the Eyring model or the Mungall model is not too far off with the largest difference no more than 1 order of magnitude. However, predicting SiO_2 diffusivity from viscosity is not as good as using eq 5.

4.2. SiO_2 Concentration at Quartz Saturation. The interface SiO_2 concentration (C_0) during quartz dissolution in every experiment is extracted from fitted profile as the extrapolated concentration at $x = 0$ (Table 3). The interface SiO_2 concentrations at a given temperature and pressure are roughly independent of the experimental duration within experimental uncertainty (Figure 4a,b). That is, quartz dissolution is diffusion-controlled, and the interface melt composition can be approximately regarded as the equilibrium composition of the melt with quartz.

SiO_2 content plays the dominant role for quartz saturation, while other components play minor roles through their effect on the activity coefficient of SiO_2 in the melt. SiO_2 activity (equaling activity coefficient times concentration) in the melt equilibrated with quartz at the same temperature must be the same. However, SCQS (silica concentration at quartz saturation) is different between rhyolitic or basaltic melts at the same temperature and pressure (Table 3). For example, at 1300 °C and 0.5 GPa, SCQS is between 83.0 and 85.6 wt % (the range is regarded as experimental and extrapolation uncertainty) when the initial melt is rhyolite, but between 71.5 and 73.5 wt % if the initial melt is basalt. Note that the interface melts (saturation melts) in both cases are rhyolitic with the former containing significantly lower FeO, MgO, and CaO but higher K_2O (Table 3). The higher SiO_2 concentration for quartz saturation in the former by (84.3/72.5 − 1) = 16% than in the latter means that SiO_2 activity coefficient in the former interface melt (lower FeO, MgO, and CaO but significantly higher K_2O) is smaller by 16%. The effect of other components on SiO_2 activity coefficient accounts for the difference in SCQS.

The rhyolite−MELTS software package[12,13] is used to calculate the liquidus based on the interface melt compositions we obtained. Note that these melts contain high SiO_2 concentrations up to 95 wt %, which are likely beyond the applicability range of the rhyolite-MELTS software. Given the interface melt composition, the rhyolite-MELTS software correctly predicts the liquidus phase to be quartz, but the calculated liquidus temperatures are higher than the experimental temperatures by 140 to 296 °C when the initial melt is rhyolitic, and by −92 to 142 °C when the initial melt

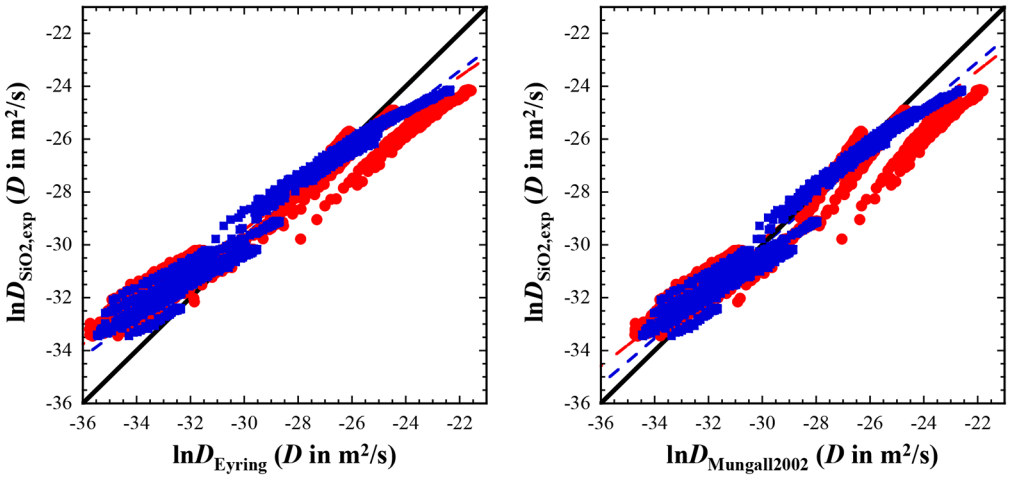

Figure 9. Comparison of experimental SiO_2 EBDC with Eyring diffusivity and with diffusivity calculated using the tracer diffusivity model for high-field strength elements by Mungall.[62] In calculating D values, the viscosity models of ref 63 (red circles) and ref 64 (blue squares) are used. The heavy solid line is 1:1 line.

DOI: 10.1021/acsearthspacechem.8b00193
ACS Earth Space Chem. 2019, 3, 599−616

is basaltic. The large difference even when the interface SiO_2 concentration is 71−85 wt % means that there is much room for improvement of the rhyolite−MELTS, and our data on SCQS at various temperatures (Table 3) can provide important constraints for improvement of thermodynamic models of silicate melts.[9−13,65]

Before such improvement is available, there is a need to develop a simple and practical way to approximate the quartz−melt equilibrium for the purpose of quantifying quartz dissolution and growth kinetics. We relate the SiO_2 wt % concentration in the interface melt with the experimental temperature for different melt systems (Figure 10). Because

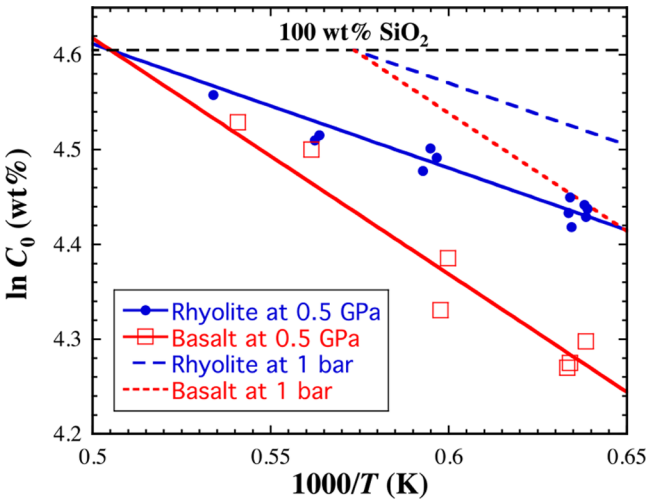

Figure 10. SiO_2 concentration at β-quartz saturation (that is, interface SiO_2 concentration, Table 3) versus $1000/T$ with linear regression lines. SiO_2 (100 wt %) is marked by the dashed horizontal line. Blue solid circles are for quartz dissolution in molten rhyolite at 0.5 GPa; red open squares are for quartz dissolution in molten basalt at 0.5 GPa. The blue long-dashed line is the estimated ln C_0 versus $1000/T$ relation at 1 bar in rhyolite, and the red short-dashed line is that in basalt.

the interface SiO_2 concentration (C_0) is an apparent equilibrium constant, we express $\ln C_0 = A - B/T$ where $B \sim \Delta H/R$ with ΔH being the standard enthalpy of the reaction $SiO_2(\beta\text{-qz}) \rightleftharpoons SiO_2(\text{melt})$, and R being the universal gas constant. Because we are using concentrations rather than chemical activities and because the activity coefficient depends on the concentrations of other components, A and B may vary from rhyolite to basalt. An important constraint is the melting temperature of β-quartz at 0.5 GPa (1707 °C, ref 39), meaning C_0 = 100% at the temperature. Hence, we construct the β-quartz-melt equilibrium relation at 0.5 GPa for rhyolite and basalt respectively forcing each to go through C_0 = 100% at 1980.15 K (solid blue and red lines in Figure 10)

$$\text{In rhyolite at 0.5 GPa:} \quad \ln C_0 = 5.267 - 1310/T, \quad r^2 = 0.916, \tag{7a}$$

$$\text{In basalt at 0.5 GPa:} \quad \ln C_0 = 5.862 - 2489/T, \quad r^2 = 0.933 \tag{7b}$$

where C_0 is SiO_2 concentration in wt % in the interface melt (that is, SCQS). When using the experimental temperature to predict the experimental interface SiO_2 concentration, the largest error is 1.9 wt % using eq 7a (or 0.02 in lnC_0) when the initial melt is rhyolitic, and 3.4 wt % using eq 7b (or 0.04 in lnC_0) when the initial melt is basaltic. When using the experimental interface SiO_2 concentration to predict the experimental temperature, the largest error is 48 °C for both eq 7a when the initial melt is rhyolitic and eq 7b when the initial melt is basaltic. These prediction errors are significantly smaller than those from the calculation of the rhyolite-MELTS package (Gualda et al., 2012; Ghiorso et al., 2015).

Note that although the variation of diffusivity in silicate melts with pressure is often negligible for a pressure interval of 1 GPa (e.g., ref 15), the saturation concentration C_0 depends on pressure more strongly than diffusivity.[15] For example, the metastable equilibrium temperature between β-quartz and pure SiO_2 melt is 1707 °C at 0.5 GPa and 1471 °C at 1 bar (ref 39), varying by 236 °C in 0.5 GPa pressure interval. To estimate the ln C_0 versus $1/T$ relation at 1 bar, we use the metastable equilibrium temperature between β-quartz and pure SiO_2 melt at 1 bar, meaning that the line must pass through the point of (1000/1744.15, ln 100), and ignore the variation of B in eqs 7a and 7b in the pressure range of 1 bar to 0.5 GPa, leading to

$$\text{In rhyolite at 1 bar:} \quad \ln C_0 \approx 5.356 - 1310/T \tag{7c}$$

$$\text{In basalt at 1 bar:} \quad \ln C_0 \approx 6.032 - 2489/T \tag{7d}$$

These two rough equations are shown as dashed blue and red lines in Figure 10.

4.3. Diffusive Mineral Dissolution Rates for Concentration-Dependent *D*. For diffusive crystal dissolution when the diffusivity of the principal equilibrium-determining component is constant across the concentration profile, the melt growth distance can be expressed by the parabolic relation[2]

$$L_{\text{melt}} = 2\alpha\sqrt{Dt} \tag{8}$$

where α is determined using eq 2 from the concentrations of the principal equilibrium-determining component in the interface melt (C_0), far-field melt (C_∞), and the mineral (C_c). In the case of quartz dissolution, the diffusivity of SiO_2 (the equilibrium-determining component) is not constant. No theory is currently available to estimate diffusive crystal dissolution rate (or melt growth rate) when the diffusivity depends on concentration. For example, Yang et al.[17] showed that Sn diffusion during cassiterite dissolution is concentration dependent, but there were not enough data to develop a predictive theory for mineral dissolution rate or melt growth rate. This section uses an empirical approach to address how the melt growth distance or mineral dissolution distance can be estimated when D depends on concentration.

It has been shown using Boltzmann analysis that even when D depends on concentration, the concentration profile still propagates according to $\sqrt{t}$, and during mineral dissolution the melt growth distance is still proportional to $\sqrt{t}$ (Appendix A). Experimental data are consistent with this expectation. For example, Figure 4c,d also shows that quartz dissolution distance is proportional to $\sqrt{t}$. In addition, even though H_2O diffusivity in silicate melts depends on its concentration,[66,67] dehydration mass loss when the far-field composition has not changed is also proportional to $\sqrt{t}$ (refs 68 and 69). Hence, in modeling the melt growth distance during quartz dissolution in silicate melts, we adopt the formulation of eq 8 with α solved from eq 2 but interpreting the constant D in the equation to be an effective diffusivity, D_{eff}, leading to

DOI: 10.1021/acsearthspacechem.8b00193
ACS Earth Space Chem. 2019, 3, 599−616

$$L_{melt} = 2\alpha\sqrt{D_{eff}t} \quad (9)$$

Equation 9 leads to

$$D_{eff} = \frac{L_{melt}^2}{4\alpha^2 t} \quad (10)$$

D_{eff} values so calculated are listed in Table 4. Because D_{eff} is an effective diffusivity across the entire concentration profile, one might expect that it may be expressed as a combination of the diffusivities at the interface melt and the far-field melt. In Figure 11, $\ln(D_{eff}/D_{farfield})$ versus $\ln(D_{interface}/D_{farfield})$ are

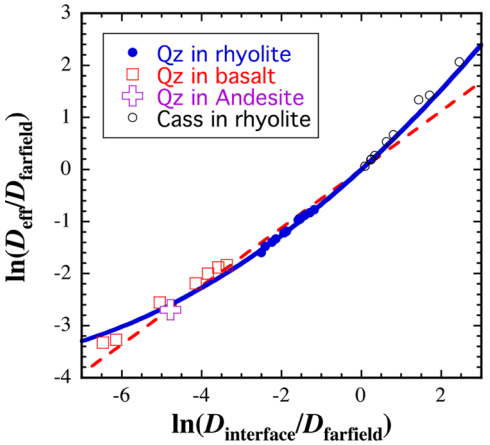

Figure 11. Relating effective diffusivity (D_{eff}) for mineral dissolution to diffusivity at the far-field and interface melts. Quartz dissolution data in molten rhyolite and basalt are from this work. Quartz dissolution experiment in molten andesite is from ref 2. Cassiterite dissolution experiments in molten rhyolite are from ref 17. The red dashed line is a linear fit passing through the origin (eq 11); and the blue solid curve is a second order polynomial fit passing through the origin (eq 12).

plotted, including SiO_2 diffusivity data in Table 4, SiO_2 diffusivity obtained from exp #234 of ref 2 using concentration-dependent D_{SiO_2} (eq 4), and Sn diffusivity data during cassiterite dissolution in rhyolitic melt.[17] For the case of cassiterite dissolution, Sn rather than SiO_2 diffusion data are used because Sn is the principal equilibrium-determining component for cassiterite saturation.

The data in Figure 11 show some curvature. For simplicity, a first order linear fit with an intercept of zero (red dashed line) is carried out to obtain $k = 0.560 \pm 0.015$ with $r^2 = 0.9708$

$$D_{eff} \approx (D_{interface})^{0.56}(D_{farfield})^{0.44} \quad (11)$$

To account for the curvature, a curve fit (blue solid curve in Figure 11) is obtained by forcing the intercept to be zero

$$\ln\frac{D_{eff}}{D_{farfield}} = \left(0.6996 + 0.0327\cdot\ln\frac{D_{interface}}{D_{farfield}}\right)\ln\frac{D_{interface}}{D_{farfield}} \quad (12)$$

with $r^2 = 0.9927$. In both fits, the intercept is forced to be zero because $\ln(D_{interface}/D_{farfield}) = 0$ means constant D, indicating that $\ln(D_{eff}/D_{farfield})$ must be zero. Work is currently in progress through systematic numerical simulations to derive a general relation for predicting diffusive mineral dissolution or growth rate when the diffusivity is concentration dependent.[70]

Once D_{eff} is predicted, the melt growth distance L during quartz and cassiterite dissolution may be calculated using eq 9, with α from eq 2 and t being the experimental duration. When α is positive, the melt grows (the crystal dissolves). When α is negative, the melt is consumed, and the crystal grows. Worked numerical examples are given in the supplementary files to help readers to use the method.

4.4. Convective Dissolution Rates. For modeling convective dissolution or growth rates of a rising bubble or sinking/rising crystal when diffusivity varies significantly, as a first order approximation, we suggest using similar approaches as in refs 71−73 but replacing the constant D by D_{eff} and the boundary layer thickness by e-folding thickness δ_{eff} (the distance in the melt from the mineral−melt interface at which the concentration equals $C_0/e + C_\infty(1 - 1/e)$ where $e = 2.71828...$). The use of e-folding distance avoids the need to find the very steep slope of the concentration profile at the mineral−melt interface. Hence, the general equation for predicting convective melt growth rate[2] becomes

$$V = \frac{D_{eff}}{\delta_{eff}}\frac{(C_0 - C_\infty)}{(C_c - C_0)} \quad (13)$$

Watson[1] investigated dynamic quartz dissolution in a basaltic melt (containing 49.5 wt % SiO_2) at 1300 and 1400 °C and 1 bar by rotating a cage with a quartz crystal in a bucket of melt at three rotations per minute. He measured oxide concentration profiles and found extremely steep concentration slope near the interface. He estimated the boundary layer thickness to be 75 μm. He also estimated quartz dissolution rate of 1.5×10^{-6} g/cm^2/s = 0.0059 μm/s at 1300 °C and 3.3×10^{-6} g/cm^2/s = 0.013 μm/s at 1400 °C. This is a case of quartz dissolution with forced convection. The SiO_2 concentration in the interface melt at 1300 °C and 1 bar is very roughly estimated from eq 7d to be 85.61 wt %, which is between the extrapolated values of the three experiments at 1300 °C (ref 1). Hence, $(C_0 - C_\infty)/(C_c - C_0) = (85.61 - 49.5)/(100 - 85.61) \approx 2.51$. Because diffusivities are not expected to change much in a 0.5 GPa interval,[15,16] we use eq 6b and obtain $D_{farfield} = 6.41$ μm^2/s, and $D_{interface} = 0.0215$ μm^2/s. Note the huge difference in $D_{farfield}$ and $D_{interface}$, by a factor of 300, consistent with the extremely steep slope near the interface in ref 1. Estimated $D_{eff} = 0.344$ μm^2/s using eq 12. The predicted melt growth rate using eq 13 is 0.0115 μm/s, and quartz dissolution rate is 0.0126 μm/s. Experimental quartz dissolution rate at 1300 °C is 0.0059 μm/s (ref 1). The predicted value is about 2 times the observed value. Considering the roughness in estimating C_0 and δ, this level of agreement is deemed acceptable.

5. CONCLUSIONS

1. Quartz dissolution kinetics in rhyolitic and basaltic melts is complicated because the SiO_2 concentration profile cannot be described by a constant diffusivity. We assessed the dependence of SiO_2 diffusivity as a function of melt composition (including H_2O concentration) and temperature and developed a method to predict mineral dissolution rate for the case of concentration-dependent diffusivity.

2. The compositional dependence of D_{SiO_2}, including the effect of H_2O, can be roughly captured by an exponential dependence of D_{SiO_2} on the cation mole fraction of Si + Al. The dependence of D_{SiO_2} on Si + Al becomes weaker as

DOI: 10.1021/acsearthspacechem.8b00193
ACS Earth Space Chem. 2019, 3, 599−616

temperature increases. D_{SiO_2} during quartz dissolution in molten rhyolite, andesite and basalt can be roughly accounted for using a simple model (eq 5) with maximum error of 0.95 ln D units. The effects of other components are small and cannot be resolved yet. D_{SiO_2} is related to viscosity but using viscosity to predict D_{SiO_2} has larger errors than using eq 5.

3. We developed a method to predict diffusive mineral dissolution distance in melts when the diffusivity is concentration-dependent. The mineral dissolution distance can be estimated using $L = 2\alpha\sqrt{D_{eff}t}(\rho_{melt}/\rho_{mineral})$ where D_{eff} is the effective diffusivity of the principal equilibrium-determining component across the concentration profile and can be estimated from D in the far-field and interface melts. The approach works well for both quartz dissolution and cassiterite dissolution.

4. For predicting convective mineral dissolution rate, we propose to use D_{eff} to replace the constant D in existing literature treatments.

5. We derived the equation for using Boltzmann analysis to treat concentration-dependent diffusivity from diffusion profiles generated by diffusive crystal dissolution.

APPENDIX A

Boltzmann Analysis for Diffusion during Crystal Dissolution

Diffusion equation of mineral dissolution in the melt in the interface-fixed reference frame can be written as

$$\frac{\partial C}{\partial t} = \frac{\partial}{\partial x}\left(D\frac{\partial C}{\partial x}\right) - V\frac{\partial C}{\partial x} \tag{A1}$$

with initial and boundary conditions

$$C|_{t=0} = C_\infty$$

$$\left(D\frac{\partial C}{\partial x}\right)\Big|_{x=0} + V(C_c - C_{x=0}) = 0 \tag{A2}$$

Using Boltzmann transformation

$$\eta = \frac{x}{\sqrt{t}}; \quad \frac{\partial \eta}{\partial x} = \frac{1}{\sqrt{t}}; \quad \frac{\partial \eta}{\partial t} = -\frac{\eta}{2t} \tag{A3}$$

Transform the diffusion equation using η

$$-\frac{\eta}{2t}\frac{\partial C}{\partial \eta} = \frac{1}{t}\left[\frac{\partial}{\partial \eta}\left(D\frac{\partial C}{\partial \eta}\right)\right] - \frac{V}{\sqrt{t}}\frac{\partial C}{\partial \eta} \tag{A4}$$

$$V(C_c - C_{x=0}) + \frac{1}{\sqrt{t}}\left(D\frac{\partial C}{\partial \eta}\right)\Big|_{\eta=0} = 0 \tag{A5}$$

When diffusion control is reached, $C|_{x=0}$ is a constant, and $D\partial C/\partial\eta$ at $\eta = 0$ is a constant. Hence, V is inversely proportional to $\sqrt{t}$ and may be written as $B//\sqrt{t}$.

Substitute V from eq A5 into the diffusion eq A4

$$-\frac{\eta}{2}\frac{\partial C}{\partial \eta} = \left[\frac{\partial}{\partial \eta}\left(D\frac{\partial C}{\partial \eta}\right)\right] + \frac{\left(D\frac{\partial C}{\partial \eta}\right)\Big|_{\eta=0}}{C_c - C_{\eta=0}}\frac{\partial C}{\partial \eta} \tag{A6}$$

Rearrange the above equation (note that $D|_{n=0}$ is a constant)

$$\left[\frac{\left(D\frac{\partial C}{\partial \eta}\right)\Big|_{\eta=0}}{C_c - C_{\eta=0}} + \frac{\eta}{2}\right]\frac{\partial C}{\partial \eta} + \left[\frac{\partial}{\partial \eta}\left(D\frac{\partial C}{\partial \eta}\right)\right] = 0 \tag{A7}$$

Integrate the above differential equation along η from η_0 to ∞ and recognizing $(\partial C/\partial\eta)_{\eta=\infty} = 0$

$$\frac{\left(D\frac{\partial C}{\partial \eta}\right)\Big|_{\eta=0}}{C_c - C_{\eta=0}}(C_\infty - C_{\eta_x}) + \frac{1}{2}\int_{C_{\eta_x}}^{C_\infty}\eta\, dC - D\frac{\partial C}{\partial \eta}\Big|_{\eta_x} = 0 \tag{A8}$$

Solving D from the above equation leads to

$$D = \frac{\frac{\left(D\frac{\partial C}{\partial \eta}\right)\Big|_{\eta=0}}{C_c - C_{\eta=0}}(C_\infty - C_{\eta_x}) + \frac{1}{2}\int_{C_{\eta_x}}^{C_\infty}\eta\, dC}{\frac{\partial C}{\partial \eta}\Big|_{\eta_x}} = \frac{\left(D\frac{\partial C}{\partial x}\right)\Big|_{x=0}\frac{(C_\infty - C_x)}{C_c - C_{x=0}} + \frac{1}{2t}\int_{C_x}^{C_\infty}x dC}{\frac{\partial C}{\partial x}\Big|_x} \tag{A9}$$

When $x = 0$, $D = D|_{x=0}$, meaning

$$D_{x=0} = \frac{C_c - C_0}{C_c - C_\infty}\frac{\int_{C_0}^{C_\infty}x\, dC}{2t\frac{\partial C}{\partial x}\Big|_{x=0}} \tag{A10}$$

Substitute $D|_{x=0}$ into eq A9

$$D = \frac{\frac{C_\infty - C_x}{C_c - C_\infty}\int_{C_0}^{C_\infty}x\, dC + \int_{C_x}^{C_\infty}x\, dC}{2t\frac{\partial C}{\partial x}\Big|_x}, \quad t > 0 \tag{A11}$$

Hence, to calculate D at a given point x, we need C_x, $(\partial C/\partial x)_x$, $\int x\, dC$ from C_x to C_∞. Other parameters in the above equation are constants for a given experiment and a given profile.

ASSOCIATED CONTENT

Supporting Information

The Supporting Information is available free of charge on the ACS Publications website at DOI: 10.1021/acsearthspacechem.8b00193.

Appendix B including worked numerical examples for calculating diffusive dissolution distance; MatLab code for carrying out Boltzmann analysis; SiO_2 concentration profile with fits in every experiment (PDF)

Electron microprobe data for quartz dissolution experiments in rhyolite (XLSX)

Electron microprobe data for quartz dissolution experiments in basalt (XLSX)

AUTHOR INFORMATION

Corresponding Author

*E-mail address: youxue@umich.edu

ORCID

Youxue Zhang: 0000-0002-7439-0086

Notes

The authors declare no competing financial interest.

DOI: 10.1021/acsearthspacechem.8b00193
ACS Earth Space Chem. 2019, 3, 599−616

■ ACKNOWLEDGMENTS

This research is supported by NSF Grants EAR-1019440, EAR-1524473, and EAR-1829822. Electron microprobe work is carried out on a Cameca SX100 instrument at Electron Microbeam Analysis Laboratory of the University of Michigan, which is supported by NSF grant EAR-9911352. We thank Sumit Chakraborty, Yan Liang, F. J. Ryerson, and three anonymous reviewers for their comments.

■ REFERENCES

(1) Watson, E. B. Basalt contamination by continental crust: some experiments and models. *Contrib. Mineral. Petrol.* **1982**, *80*, 73−87.
(2) Zhang, Y.; Walker, D.; Lesher, C. E. Diffusive crystal dissolution. *Contrib. Mineral. Petrol.* **1989**, *102*, 492−513.
(3) Liang, Y. Diffusive dissolution in ternary systems: analysis with applications to quartz and quartzite dissolution in molten silicates. *Geochim. Cosmochim. Acta* **1999**, *63*, 3983−3995.
(4) Shaw, C. S. J. The effect of experiment geometry on the mechanism and rate of dissolution of quartz in basanite at 0.5 GPa and 1350 °C. *Contrib. Mineral. Petrol.* **2000**, *139*, 509−525.
(5) Shaw, C. S. J. Mechanisms and rates of quartz dissolution in melts in the CMAS (CaO-MgO-Al_2O_3-SiO_2) system. *Contrib. Mineral. Petrol.* **2004**, *148*, 180−200.
(6) Shaw, C. S. J. Effects of melt viscosity and silica activity on the rate and mechanism of quartz dissolution in the melts of the CMAS and CAS systems. *Contrib. Mineral. Petrol.* **2006**, *151*, 665−680.
(7) Shaw, C. S. J. The effects of potassium addition on the rate of quartz dissolution in the CMAS and CAS systems. *Contrib. Mineral. Petrol.* **2012**, *164*, 839−857.
(8) Acosta-Vigil, A.; London, D.; Morgan, G. B., VI; Dewers, T. A. Dissolution of quartz, albite, and orthoclase in H_2O-saturated haplogranitic melt at 800°C and 200 MPa: diffusive transport properties of granitic melts at crustal anatectic conditions. *J. Petrol.* **2006**, *47*, 231−254.
(9) Ghiorso, M. S.; Sack, R. O. Chemical mass transfer in magmatic processes, IV: a revised and internally consistent thermodynamic model for the interpolation and extrapolation of liquid-solid equilibria in magmatic systems at elevated temperatures and pressures. *Contrib. Mineral. Petrol.* **1995**, *119*, 197−212.
(10) Ghiorso, M. S.; Hirschmann, M. M.; Reiners, P. W.; Kress, V. C. The pMELTS: A revision of MELTS for improved calculation of phase relations and major element partitioning related to partial melting of the mantle to 3 GPa. *Geochem., Geophys., Geosyst.* **2002**, *3*, 1−35.
(11) Asimow, P. D.; Ghiorso, M. S. Algorithmic modifications extending MELTS to calculate subsolidus phase relations. *Am. Mineral.* **1998**, *83*, 1127−1132.
(12) Gualda, G. A. R.; Ghiorso, M. S.; Lemons, R. V.; Carley, T. L. Rhyolite-MELTS: a modified calibration of MELTS optimized for silica-rich, fluid-bearing magmatic systems. *J. Petrol.* **2012**, *53*, 875−890.
(13) Ghiorso, M. S.; Gualda, G. A. R. An H_2O-CO_2 mixed fluid saturation model compatible with rhyolite-MELTS. *Contrib. Mineral. Petrol.* **2015**, *169*, 53.
(14) Zhang, Y. *Geochemical Kinetics*; Princeton University Press: Princeton, NJ, 2008; p 664.
(15) Chen, Y.; Zhang, Y. Olivine dissolution in basaltic melt. *Geochim. Cosmochim. Acta* **2008**, *72*, 4756−4777.
(16) Chen, Y.; Zhang, Y. Clinopyroxene dissolution in basaltic melt. *Geochim. Cosmochim. Acta* **2009**, *73*, 5730−5747.
(17) Yang, Y.; Zhang, Y.; Simon, A.; Ni, P. Cassiterite dissolution and Sn diffusion in silicate melts of variable water content. *Chem. Geol.* **2016**, *441*, 162−176.
(18) Yu, Y.; Zhang, Y.; Chen, Y.; Xu, Z. Kinetics of anorthite dissolution in basaltic melt. *Geochim. Cosmochim. Acta* **2016**, *179*, 257−274.
(19) Zhang, Y.; Xu, Z. Zircon saturation and Zr diffusion in rhyolitic melts, and zircon growth geospeedometer. *Am. Mineral.* **2016**, *101*, 1252−1267.
(20) Cooper, A. R., The use and limitations of the concept of an effective binary diffusion coefficient for multi-component diffusion. In *Mass Transport in Oxides*; Wachman, J. B., Franklin, A. D., Eds.; Nat. Bur. Stand. Spec. Publ., 1968; Vol. *296*, pp 79−84.
(21) Lesher, C. E.; Walker, D. Solution properties of silicate liquids from thermal diffusion experiments. *Geochim. Cosmochim. Acta* **1986**, *50*, 1397−1411.
(22) Baker, D. R.; Watson, E. B. Diffusion of major and trace elements in compositionally complex Cl- and F-bearing silicate melts. *J. Non-Cryst. Solids* **1988**, *102*, 62−70.
(23) Koyaguchi, T. Chemical gradient at diffusive interfaces in magma chambers. *Contrib. Mineral. Petrol.* **1989**, *103*, 143−152.
(24) Baker, D. R. Chemical interdiffusion of dacite and rhyolite: anhydrous measurements at 1 atm and 10 kbar, application of transition state theory, and diffusion in zoned magma chambers. *Contrib. Mineral. Petrol.* **1990**, *104*, 407−423.
(25) Baker, D. R. Interdiffusion of hydrous dacitic and rhyolitic melts and the efficacy of rhyolite contamination of dacitic enclaves. *Contrib. Mineral. Petrol.* **1991**, *106*, 462−473.
(26) Baker, D. R.; Bossanyi, H. The combined effect of F and H_2O on interdiffusion between peralkaline dacitic and rhyolitic melts. *Contrib. Mineral. Petrol.* **1994**, *117*, 203−214.
(27) Van der Laan, S. R.; Zhang, Y.; Kennedy, A.; Wylie, P. J. Comparison of element and isotope diffusion of K and Ca in multicomponent silicate melts. *Earth Planet. Sci. Lett.* **1994**, *123*, 155−166.
(28) Lesher, C. E.; Hervig, R. L.; Tinker, D. Self diffusion of network formers (silicon and oxygen) in naturally occurring basaltic liquid. *Geochim. Cosmochim. Acta* **1996**, *60*, 405−413.
(29) Liang, Y.; Richter, F. M.; Davis, A. M.; Watson, E. B. Diffusion in silicate melts, I: self diffusion in CaO-Al_2O_3-SiO_2 at 1500°C and 1 GPa. *Geochim. Cosmochim. Acta* **1996**, *60*, 4353−4367.
(30) Liang, Y.; Richter, F. M.; Watson, E. B. Diffusion in silicate melts, II: multicomponent diffusion in CaO-Al_2O_3-SiO_2 at 1500°C and 1 GPa. *Geochim. Cosmochim. Acta* **1996**, *60*, 5021−5035.
(31) Tinker, D.; Lesher, C. E. Self diffusion of Si and O in dacitic liquid at high pressures. *Am. Mineral.* **2001**, *86*, 1−13.
(32) Tinker, D.; Lesher, C. E.; Hucheon, I. D. Self-diffusion of Si and O in diopside-anorthite melt at high pressures. *Geochim. Cosmochim. Acta* **2003**, *67*, 133−142.
(33) Macris, C. A.; Asimow, P. D.; Badro, J.; Eiler, J. M.; Zhang, Y.; Stolper, E. M. Seconds after impact: insights into the thermal history of impact ejecta from diffusion between lechateliertite and host glass in tektites and experiments. *Geochim. Cosmochim. Acta* **2018**, *241*, 69−94.
(34) Zhang, Y.; Ni, H.; Chen, Y. Diffusion data in silicate melts. *Rev. Mineral. Geochem.* **2010**, *72*, 311−408.
(35) Dixon, J. E.; Clague, D. A.; et al. Gabbroic xenoliths and host ferrobasalt from the southern Juan de Fuca Ridge. *J. Geophys. Res.* **1986**, *91*, 3795−3820.
(36) Dixon, J. E.; Stolper, E. M.; Delaney, J. R. Infrared spectroscopic measurements of CO_2 and H_2O in Juan de Fuca Ridge basaltic glasses. *Earth Planet. Sci. Lett.* **1988**, *90*, 87−104.
(37) Newman, S.; Stolper, E. M.; Epstein, S. Measurement of water in rhyolitic glasses: calibration of an infrared spectroscopic technique. *Am. Mineral.* **1986**, *71*, 1527−1541.
(38) Hui, H.; Zhang, Y.; Xu, Z.; Behrens, H. Pressure dependence of the speciation of dissolved water in rhyolitic melts. *Geochim. Cosmochim. Acta* **2008**, *72*, 3229−3240.
(39) Hudon, P.; Jung, I. H.; Baker, D. R. Melting of β-quartz up to 2.0 GPa and thermodynamic optimization of the silica liquidus up to 6.0 GPa. *Phys. Earth Planet. Inter.* **2002**, *130*, 159−174.
(40) Ni, H.; Zhang, Y. H_2O diffusion models in rhyolitic melt with new high pressure data. *Chem. Geol.* **2008**, *250*, 68−78.
(41) Zhang, Y. A modified effective binary diffusion model. *J. Geophys. Res.* **1993**, *98*, 11901−11920.

DOI: 10.1021/acsearthspacechem.8b00193
ACS Earth Space Chem. 2019, 3, 599−616

(42) Bourova, E.; Richet, P. Quartz and cristobalite: high-temperature cell parameters and volumes of fusion. *Geophys. Res. Lett.* **1998**, *25*, 2333−2336.
(43) Kress, V. C.; Ghiorso, M. S. Multicomponent diffusion in basaltic melts. *Geochim. Cosmochim. Acta* **1995**, *59*, 313−324.
(44) Mungall, J. E.; Romano, C.; Dingwell, D. B. Multicomponent diffusion in the molten system K_2O-Na_2O-Al_2O_3-SiO_2-H_2O. *Am. Mineral.* **1998**, *83*, 685−699.
(45) Guo, C.; Zhang, Y. Multicomponent diffusion in silicate melts: SiO_2-TiO_2-Al_2O_3-MgO-CaO-Na_2O-K_2O system. *Geochim. Cosmochim. Acta* **2016**, *195*, 126−141.
(46) Guo, C.; Zhang, Y. Multicompoent diffusion in basaltic melts at 1350°C. *Geochim. Cosmochim. Acta* **2018**, *228*, 190−204.
(47) Trial, A. F.; Spera, F. J. Measuring the multicomponent diffusion matrix: experimental design and data analysis for silicate melts. *Geochim. Cosmochim. Acta* **1994**, *58*, 3769−3783.
(48) Matano, C. On the relation between the diffusion coefficient and concentrations of solid metals. *Japan J. Phys.* **1933**, *8*, 109−113.
(49) Sauer, V. F.; Freise, V. Diffusion in binaren Gemischen mit Volumenanderung. *Angew. Chem.* **1962**, *74*, 353−353.
(50) Gonzalez-Garcia, D.; Behrens, H.; Petrelli, M.; Vetere, F.; Morgavi, D.; Zhang, C.; Perugini, D. Water-enhanced interdiffusion of major elements between natural shoshonite and high-K rhyolite melts. *Chem. Geol.* **2017**, *466*, 86−101.
(51) Richter, F. M.; Davis, A. M.; DePaolo, D. J.; Watson, E. B. Isotope fractionation by chemical diffusion between molten basalt and rhyolite. *Geochim. Cosmochim. Acta* **2003**, *67*, 3905−3923.
(52) Chopra, R.; Richter, F. M.; Watson, E. B.; Scullard, C. R. Magnesium isotope fractionation by chemical diffusion in natural settings and in laboratory analogues. *Geochim. Cosmochim. Acta* **2012**, *88*, 1−18.
(53) Watson, E. B. Diffusion of cesium ions in H_2O-saturated granitic melt. *Science* **1979**, *205*, 1259−1260.
(54) Lesher, C. E.; Hervig, R. L.; Tinker, D. Self diffusion of network formers (silicon and oxygen) in naturally occurring basaltic liquid. *Geochim. Cosmochim. Acta* **1996**, *60*, 405−413.
(55) Van Orman, J. A.; Grove, T. L. Origin of lunar high-titanium ultramafic glasses: constraints from phase relations and dissolution kinetics of clinopyroxene-ilmenite cumulates. *Meteor. Planet. Sci.* **2000**, *35*, 783−794.
(56) Morgan, Z.; Liang, Y.; Hess, P. C. An experimental study of anorthosite dissolution in lunar picritic magmas: implications for crustal assimilation processes. *Geochim. Cosmochim. Acta* **2006**, *70*, 3477−3491.
(57) Baker, D. R. Tracer diffusion of network formers and multicomponent diffusion in dacitic and rhyolitic melts. *Geochim. Cosmochim. Acta* **1992**, *56*, 617−632.
(58) Baker, D. R. The effect of F and Cl on the interdiffusion of peralkaline intermediate and silicic melts. *Am. Mineral.* **1993**, *78*, 316−324.
(59) Kubicki, J. D.; Muncill, G. E.; Lasaga, A. C. Chemical diffusion in melts on the $CaMgSi_2O_6$-$CaAl_2Si_2O_8$ join under high pressures. *Geochim. Cosmochim. Acta* **1990**, *54*, 2709−2715.
(60) Lundstrom, C. C. An experimental investigation of the diffusive infiltration of alkalis into partially molten peridotite: implications for mantle melting processes. *Geochem. Geophys. Geosys.* **2003**, DOI: 10.1029/2001GC000224.
(61) Dingwell, D. B. Effects of structural relaxation on cationic tracer diffusion in silicate melts. *Chem. Geol.* **1990**, *82*, 209−216.
(62) Mungall, J. E. Empirical models relating viscosity and tracer diffusion in magmatic silicate melts. *Geochim. Cosmochim. Acta* **2002**, *66*, 125−143.
(63) Hui, H.; Zhang, Y. Toward a general viscosity equation for natural anhydrous and hydrous silicate melts. *Geochim. Cosmochim. Acta* **2007**, *71*, 403−416.
(64) Giordano, D.; Russel, J. K.; Dingwell, D. Viscosity of magmatic liquids: a model. *Earth Planet. Sci. Lett.* **2008**, *271*, 123−134.
(65) Massuyeau, M.; Gardes, E.; Morizet, Y.; Gaillard, F. A model for the activity of silica along the carbonate-kimberlite-mellilitite-basanite melt compositional joint. *Chem. Geol.* **2015**, *418*, 206−216.
(66) Shaw, H. R. Diffusion of H_2O in granitic liquids, I: experimental data; II: mass transfer in magma chambers. In *Geochemical Transport and Kinetics*; Hofmann, A. W., Giletti, B. J., Yoder, H. S., Yund, R. A., Eds.; Carnegie Institution of Washington Publ.: Washington, DC, 1974; Vol. *634*, pp 139−170.
(67) Zhang, Y.; Stolper, E. M.; Wasserburg, G. J. Diffusion of water in rhyolitic glasses. *Geochim. Cosmochim. Acta* **1991**, *55*, 441−456.
(68) Jambon, A.; Zhang, Y.; Stolper, E. M. Experimental dehydration of natural obsidian and estimation of D_{H2O} at low water contents. *Geochim. Cosmochim. Acta* **1992**, *56*, 2931−2935.
(69) Wang, L.; Zhang, Y.; Essene, E. J. Diffusion of the hydrous component in pyrope. *Am. Mineral.* **1996**, *81*, 706−718.
(70) Zhang, Y. Diffusive mineral dissolution or growth when diffusivity in the melt depends on concentration. In *Goldschmidt Conf. Abstr. 3001*; Boston, MA, U.S.A, 2018.
(71) Zhang, Y.; Xu, Z. Kinetics of convective crystal dissolution and melting, with applications to methane hydrate dissolution and dissociation in seawater. *Earth Planet. Sci. Lett.* **2003**, *213*, 133−148.
(72) Zhang, Y.; Xu, Z. "Fizzics" of bubble growth in beer and champagne. *Elements* **2008**, *4*, 47−49.
(73) Zhang, Y. Kinetics and dynamics of mass-transfer-controlled mineral and bubble dissolution or growth: a review. *Eur. J. Mineral.* **2013**, *25*, 255−266.

DOI: 10.1021/acsearthspacechem.8b00193
ACS Earth Space Chem. 2019, 3, 599−616

Kinetics of Quartz Dissolution in Natural Silicate Melts, and Dependence of SiO_2 Diffusivity on Melt Composition

Yi Yu[a] , Youxue Zhang[a,*] , Yuping Yang[b]
[a] *Department of Earth and Environmental Sciences, University of Michigan, Ann Arbor, MI, 48109, USA*
[b] *Institute of Mineral Resources, Chinese Academy of Geological Sciences, Beijing, 100037, China*
** Corresponding author. Email address: youxue@umich.edu*

Appendix B. Supporting information

1. Worked numerical examples for calculating diffusive dissolution distance when *D* depends on concentration

2. MatLab code for carrying out Boltzmann analysis to diffusion profiles during mineral dissolution

3. SiO_2 concentration profile with fits in every experiment

4. Supplementary Table 1:
   Electron microprobe data for quartz dissolution experiments in rhyolite

5. Supplementary Table 2:
   Electron microprobe data for quartz dissolution experiments in basalt

1. Worked numerical examples for calculating diffusive dissolution distance when *D* depends on concentration

Example 1. Consider quartz dissolution experiment QzDisBa101 (this study) at 1293°C for 3667 s in a basaltic melt initially containing 49.9 wt% SiO_2. Calculate the melt growth distance and compare with experimental melt growth distance L_{melt} = 29.6 μm (Table 2).

[*Solution*] First we estimate C_0 using Eq. (7b) to be 71.72 wt%. Note that C_∞ = 49.9 wt% (SiO_2 concentration in the initial melt), and $C_c \approx$ 100 wt% (SiO_2 concentration in quartz). Hence, $(C_0–C_\infty)/(C_c–C_0)$ = (71.5-49.9)/(100-71.5) = 0.7715. Solving Eq. (2) leads to α = 0.2996 (equation # means equation in the main text of this work unless otherwise indicated). Using Eq. (6b), $D_{farfield}$ = 5.70 $\mu m^2/s$, and $D_{interface}$ = 0.179 $\mu m^2/s$. The variation of D_{SiO_2} along the concentration profile is a factor of 32. Using Eq. (11), we predict $D_{eff} \approx$ 0.821 $\mu m^2/s$, and L_{melt} = 33 μm. Using Eq. (12), we predict $D_{eff} \approx$ 0.749 $\mu m^2/s$, and L_{melt} = 31 μm. Both of these predictions are in good agreement with the observed value of 29.6 μm.

Example 2. Consider cassiterite dissolution experiment CassDis1 (Yang et al., 2016) at 1100°C for 1856 s in a rhyolitic melt with negligible initial Sn concentration. The interface SnOt concentration is 12.831 wt%. Calculate the melt growth distance and compare with experimental melt growth distance L_{melt} = 2.6 μm (Table 2).

[*Solution*] First we calculate $(C_0–C_\infty)/(C_c–C_0)$ = 0.1676 where *C* is concentration of SnO_t, with C_∞ = 0, C_0 = 12.831 wt%, and C_c = 100 wt% SnO_2 = 89.382 wt% SnO_t. Solving Eq. (2) for

α leads to: $\alpha = 0.0856$. From Yang et al. (2016), $D_{farfield} = 0.0225$ $\mu m^2/s$ (Eq. 7 in Yang et al., 2016), and $D_{interface} = 0.158$ $\mu m^2/s$ using $D_{Sn} = D_{farfield}\exp(0.1561C)$ in Yang et al. (2016). Then, using Eq. (11), we predict $D_{eff} \approx 0.067$ $\mu m^2/s$, and $L_{melt} = 1.9$ μm. Using Eq. (12), we predict $D_{eff} \approx 0.100$ $\mu m^2/s$, and $L_{melt} = 2.3$ μm, fairly close to the observed value.

Note that in the above two examples, at least three uncertainties, that in predicting the interface melt composition, that in the diffusivity expression (such as Eq. (6)), and that in Eq. (12), all contribute to the error in the calculated melt growth distance. Hence, the level of agreement (within about 20% relative) in the above examples is deemed very good.

2. MatLab code for carrying out Boltzmann analysis

```
%% Main program; Boltzmann analysis of Qz dissolution profile
% Yu et al., 2019, ACS Earth & Space Chemistry
% Description; Main
% Diffusivity of SiO2 depends on concentration, varying across the profile
clear;
figure_clean();
%% Sample Number & CompNum
% Set ExpNum as 1+real ExpNum, e.g. if ExpNum is 110; then the value is set as 1110.
ExpNum = 1310;
% For quartz dissolution set CompNum = [1, 2]; for cassiterite set CompNum = [1, 3]
CompNum = [1, 2];
dx = 5; %μm
%smoothing segments
smooth_seg = [50,100];
%number of averaged points [10,25,25]
smooth_factor = [10, 25, 25];
%% load data
[Profile, ExpCond, Err] = load_data(ExpNum, CompNum);
% check loading error
if cell2mat(Err(1))
    err_info(Err);
    return;
end
%experimental conditions
[Duration, Cinf, Cc,  T] = exp_condition(ExpCond );
%fit the SiO2 and X(Si+Al) relation: 2nd order polynomial
[cxfcn, gof, op] = fit(Profile(:,2), Profile(:,3), 'poly2');
Coefs = coeffvalues(cxfcn);
fc = @(x) Coefs(1)*x.^2 + Coefs(2)*x + Coefs(3);
end
%% Smooth the data & Display the smoothed profile
ProfileSmooth = profile_smoother(Profile(:,1:2), smooth_factor,smooth_seg, dx, Cinf,
ExpNum);
%% Boltzmann Analysis & Dispaly the relation between D and C
[D_C, D_C75, V, A] = boltzmann(ProfileSmooth, Duration, Cc', Cinf', dx, ExpNum, fc);
%% export the result into files
OpFileName = strcat('./output/Boltzmann-SiO2-',num2str(ExpNum),'.csv');
OpFile = fopen(OpFileName, 'w');
%         OpContent =
[xdata(NumPoints_col(i)+1:NumPoints_col(i+1)),xdata(NumPoints_col(i)+1:NumPoints_col(i
+1))*sqrt(Duration(i)), Profile(NumPoints_col(i)+1:NumPoints_col(i+1), 1),
Profile_All(NumPoints_col(i)+1:NumPoints_col(i+1),:)]';
fprintf(OpFile, '%10s,%8s,%8s\n','SiO2 (wt%)', 'X(Si+Al)', 'lnD');
fprintf(OpFile, '%10.5f,%8.5f,%8.4f\n',D_C75');
fclose(OpFile);
```

```
function [] = figure_clean(n)
% Yu et al., 2019, ACS Earth & Space Chemistry
%figure_clean()
%Description
%When opened figures exceed the number of n (default, 3), close all figures
h = findobj('type', 'figure');
if nargin < 1
    n = 3;
end
if n == 0
    return;
else
    length(h) >= n;
```

```
    close all;
end
end



function [Profile, ExpCond, Err] = load_data(ExpNum, CompNum)
% Yu et al., 2019, ACS Earth & Space Chemistry
%[Profile, ExpCond, Err] = load_data(ExpNum, CompNum)
%Description
%load the basic data of each experiment from csv file
%load experiment conditions: T, P, duration, farfield melt comp
ExpCond = importdata('./data/Data_ExpCond.csv');
ExpCond = ExpCond.data;
ExpIdx = find(ismember(ExpCond(1,:), ExpNum));
%No sample found, return error 1
if isempty(ExpIdx)
    Err = {1, 'No such sample found'};
    Profile=[];
    ExpCond=[];
    return;
end
ExpCond = ExpCond(:,ExpIdx);
%load the concentration profiles
ProfileName = strcat('./data/Data-Profile-',num2str(ExpNum),'.csv');
Profile = importdata(ProfileName);
Profile=Profile.data;
Profile = Profile(:,[2,2+CompNum]);
Err = {0,'data loaded successfully'};
end



function [] = err_info(Err)
% Yu et al., 2019, ACS Earth & Space Chemistry
%err_info(Err)
%   report the error information regarding the different situations
fprintf(char(Err(2)));
fprintf('\n');
end



function [Duration, Cinf, Cc, T] = exp_condition(ExpCond, CompNum)
% Yu et al., 2019, ACS Earth & Space Chemistry
%[Duration, Cinf, Cc,T] = exp_condition(ExpCond)
%Description
%load the experimental duration, Qz SiO2 comp, and farfield comp
Duration = ExpCond(4);
Cinf = ExpCond(5);
Cc = ExpCond(7);
T = ExpCond(2)
end



function [ProfileSmooth] = profile_smoother(Profile, smooth_factor, smooth_seg, dx,
Cinf, ExpNum, CompNum)
% Yu et al., 2019, ACS Earth & Space Chemistry
%[Profile_s] = profile_smoother(Profile, smooth_factor, ExpNum)
%Description; Smooth the diffusion profiles without interpolation
```

```
x = Profile(:,1);
[smooth_x, ind] = unique(x);
NumPoints = ceil(max(x)/dx);
ProfileSmooth = zeros(NumPoints+2, size(Profile,2));
ProfileLen = NumPoints*dx;
% for i = 1:length(CompNum)
    y1 = smooth(x, Profile(:, 2), smooth_factor(1));
    y2 = smooth(x, Profile(:, 2), smooth_factor(2));
    y3 = smooth(x, Profile(:, 2), smooth_factor(3));
    smooth_y1 = y1(ind);
    smooth_y2 = y2(ind);
    smooth_y3 = y3(ind);
smooth_y = [smooth_y1(smooth_x<=smooth_seg(1));
smooth_y2((smooth_x>smooth_seg(1))&(smooth_x<=smooth_seg(2)));smooth_y3(smooth_x>smoot
h_seg(2))];
ProfileSmooth(:,2) = interp1(smooth_x, smooth_y, (-dx:dx:ProfileLen)',
'linear','extrap');
ProfileSmooth(:,1) = (-dx:dx:ProfileLen)';
%% visualize the smoothed profile
figure('name', strcat('Smooth Profile: ', num2str(ExpNum)));
    plot(ProfileSmooth(:,1), ProfileSmooth(:,2));
    hold on;
    scatter(Profile(:,1), Profile(:,2));
    plot([0, ProfileLen], [Cinf(1), Cinf(1)], '--r');
    hold off;
    xlim([0, max(x)]);
    title('SiO_{2}');
% end
```

```
function [D_C,D_C75, V, A] = boltzmann(Profile, Duration, Cc, Cinf, dx, ExpNum, fc)
% Yu et al., 2019, ACS Earth & Space Chemistry
%[D, V, A] = boltzmann(Profile, Duration, Cc, ExpNum, CompNum)
%Boltzmann analysis of diffusion profile, instantaneous dissolution
%rate is proportional to inverse of square root of time
%find the slope at all the points
dC_dx = diff_central(Profile(:,2), dx);  %using smoothed profile
ProfileLen = length(dC_dx);
D = zeros(ProfileLen, 1);
% calculate D0
% Area_D0 = -(trapz(Profile(2:end-1,1), Profile(2:end-1,2:end),1)-Profile(end-
1,2:end)*(ProfileLen-1)*dx);
Area_D0 = -(trapz(Profile(2:end-1,1), Profile(2:end-1,2:end),1)-Cinf*(ProfileLen-
1)*dx);
% D0 = Area_D0.*((Cc-Profile(2,2:end))./(Cc-Profile(end-
1,2:end)))./(2*Duration*dC_dx(1,:));
D0 = Area_D0.*((Cc-Profile(2,2))./(Cc-Cinf))./(2*Duration*dC_dx(1,1));
% calculate D at different C
for i = 1:ProfileLen
    %rectangle + erf curve - rectangle
    Area_i = -(Profile(i+1,2)*(i-1)*dx + trapz(Profile(1+i:end-1,1), Profile(1+i:end-
1,2),1) - (ProfileLen-1)*dx.*Cinf);
    D(i,1) = (Area_i + Area_D0.*((Cinf - Profile(1+i,2))./(Cc -
Cinf)))./(2*Duration*dC_dx(i,1));
end
D = D*(1e-12);
%instantaneous interface reaction rate
V = -D0.*dC_dx(1,1)./(Cc-Profile(2,2));
A = V*sqrt(Duration);
D_C = [Profile(2:end-1,2), D];
%% visualize the result
D_logic = (D(:,1) > 0); %& (D(:,2) > 0) & (D(:,3) > 0) & (D(:,4) > 0);
% C75_logic = Profile(2:end-1, 2) > 51;
```

```
% D_logic = (prod(D_logic*1, 2)>0)&(C75_logic);
% D_temp = D.*D_logic;
D_keep = log(D(D_logic,1));
Profile_keep = Profile(2:end-1,2);
Profile_keep = Profile_keep(D_logic,1);
Profile_keep(:,2) = fc(Profile_keep(:,1));
D_C75 = [Profile_keep, D_keep];
% D_C75 = reshape(D_C75, size(Profile_keep,1), size(Profile_keep,2)*2);
figure('name', strcat('Boltzmann Analysis: ', num2str(ExpNum)));
for j = 1:2
    subplot(2,1,j);
    scatter(Profile_keep(:,j), D_keep(:,1),'xb');
    x_limit = [min(Profile_keep(:,j)), max(Profile_keep(:,j))];
%     xlim(x_limit);
    switch j
        case 1
            title('SiO_{2}');
        case 2
            title('Si+Al mol');
    end
    %for SiO2 reverse the x axis
        set(gca, 'XDir', 'reverse');
end
end
```

Supplementary materials – fit results of SiO_2 concentration profiles

QzDisRh103

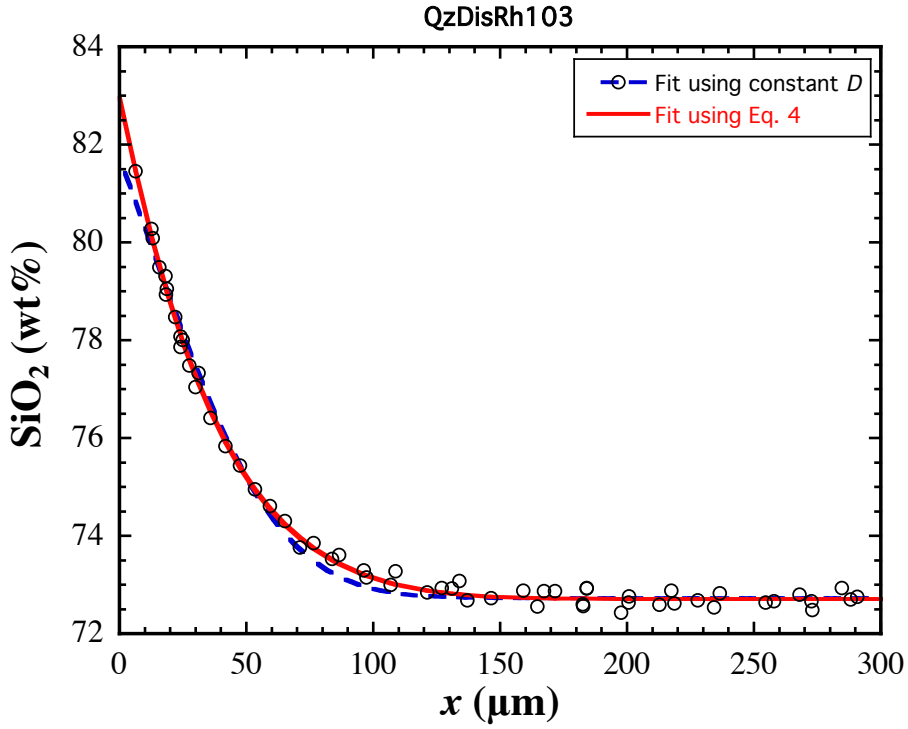

QzDisRh111

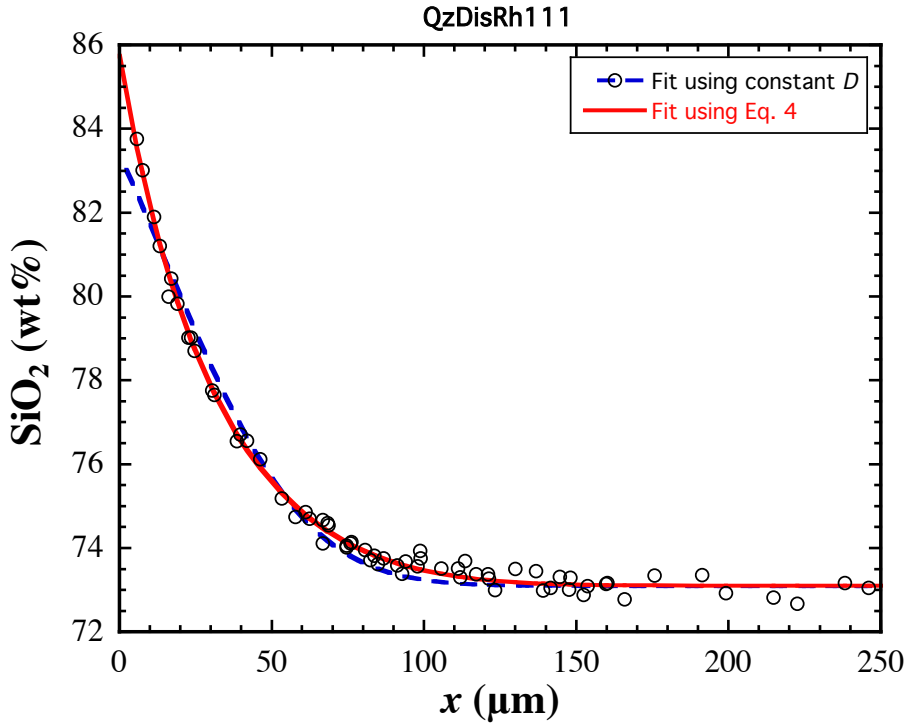

QzDisRh112

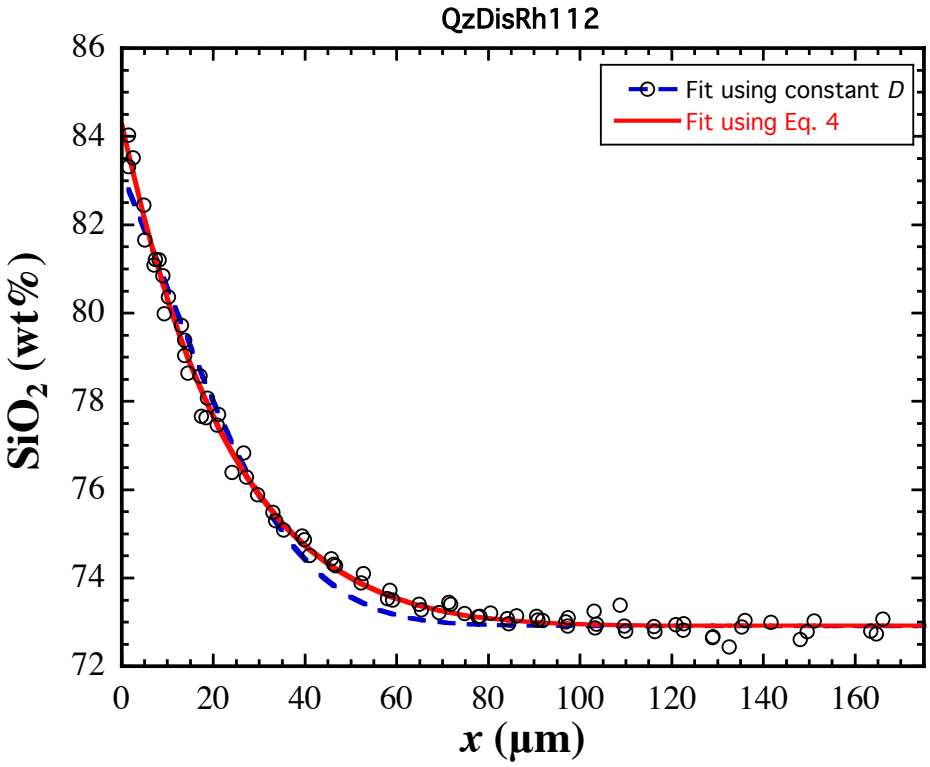

QzDisRh115

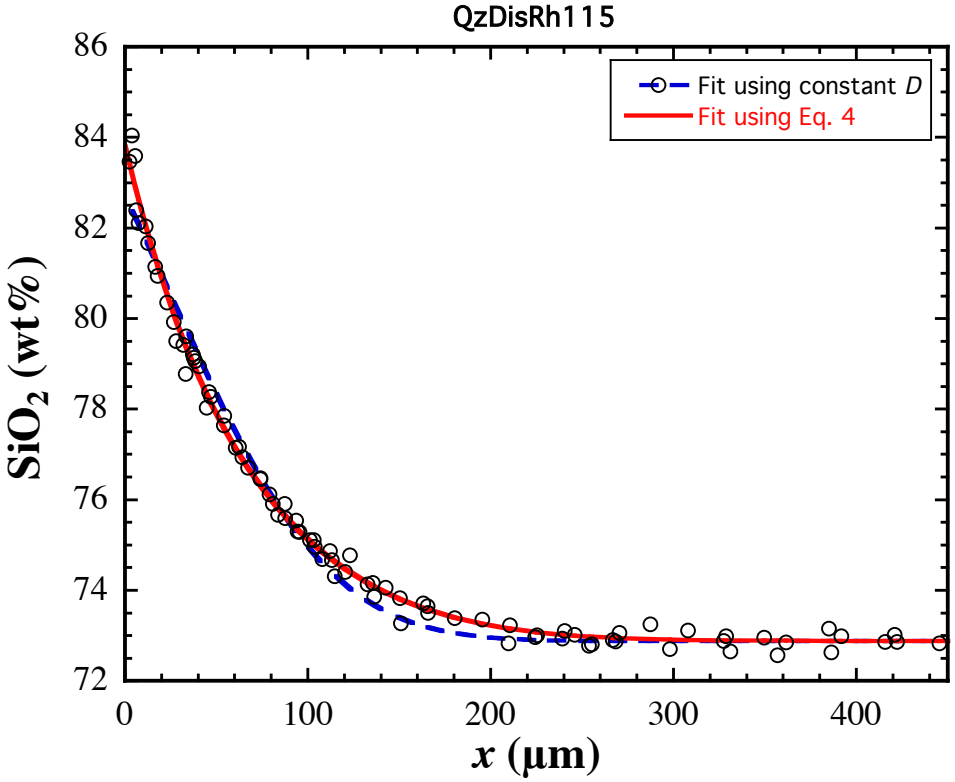

QzDisRh201

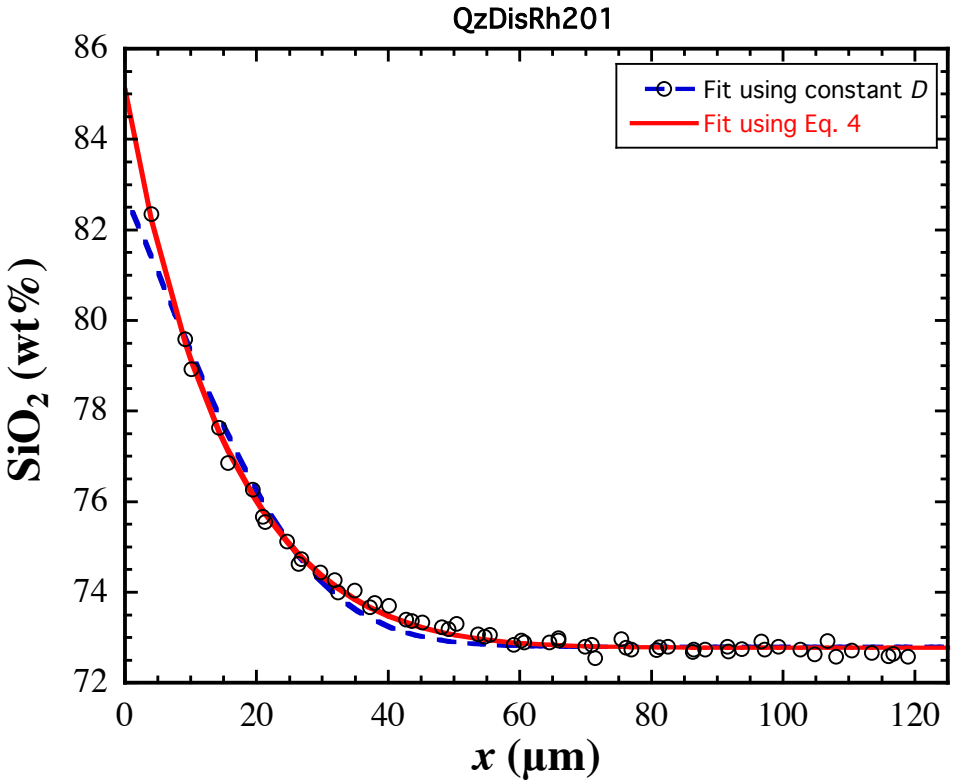

QzDisRh203

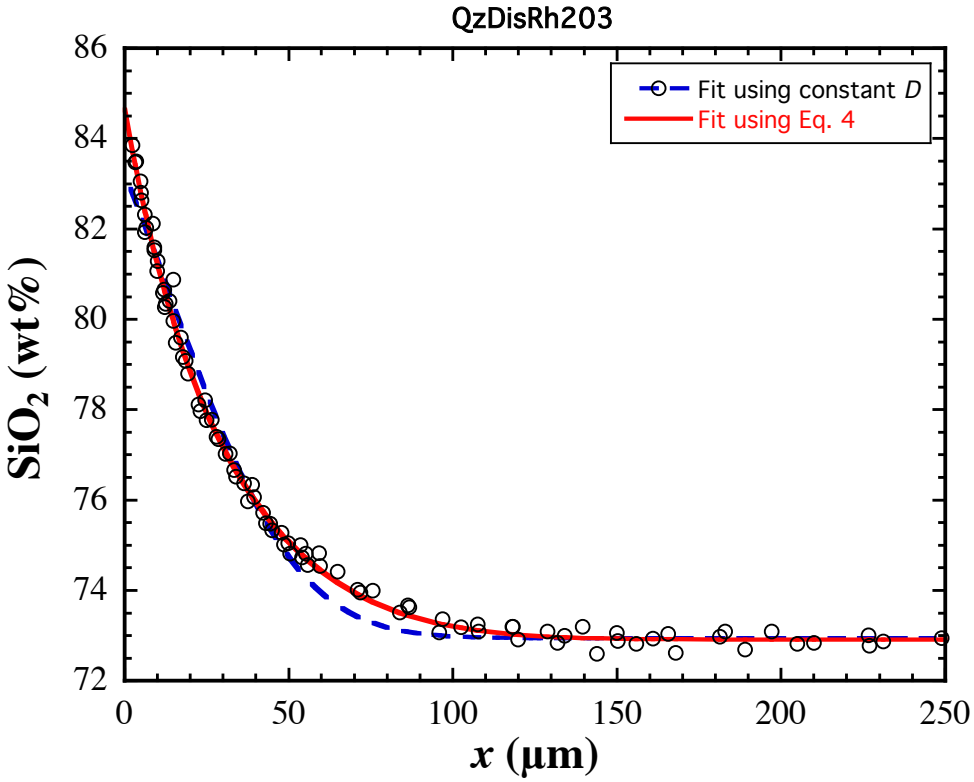

QzDisRh105

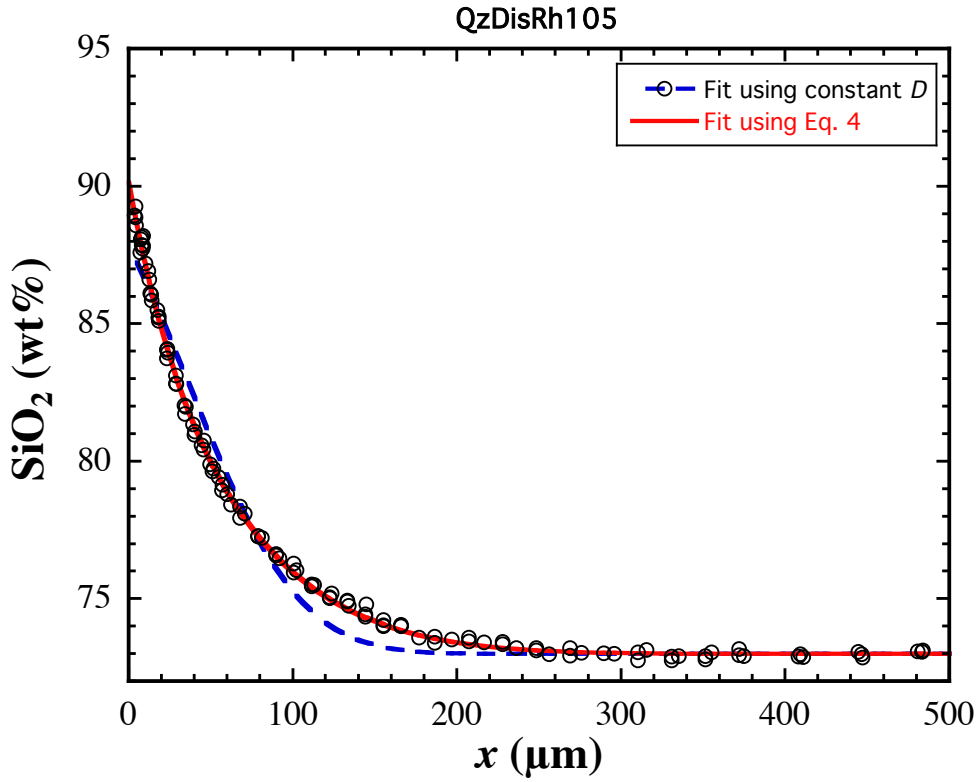

QzDisRh113

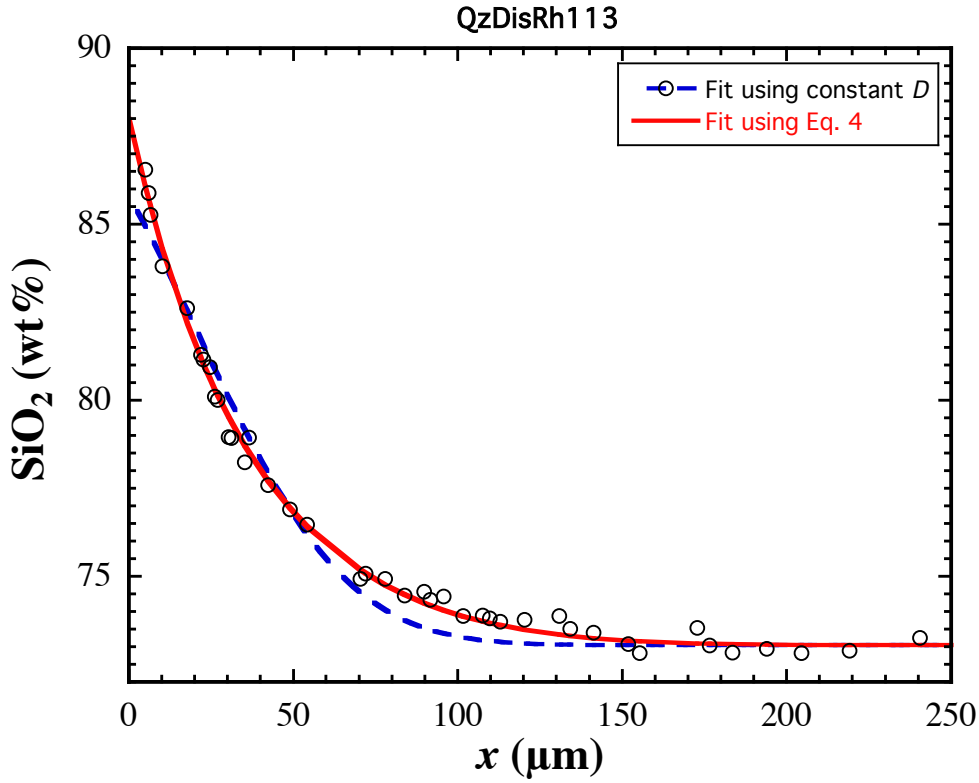

QzDisRh114

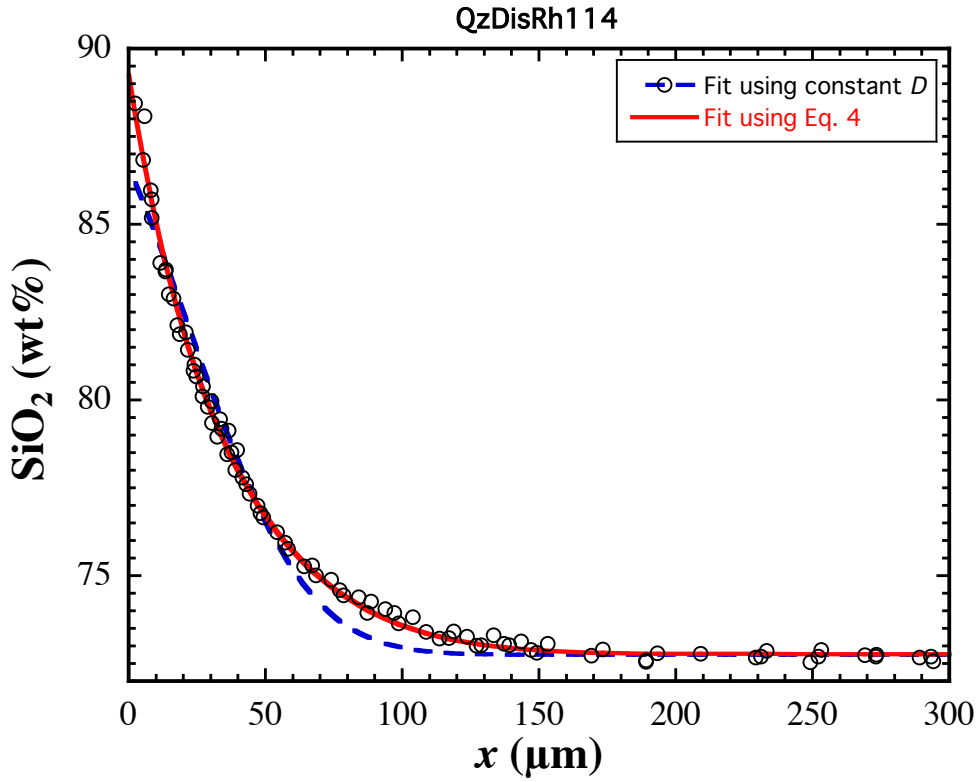

QzDisRh102

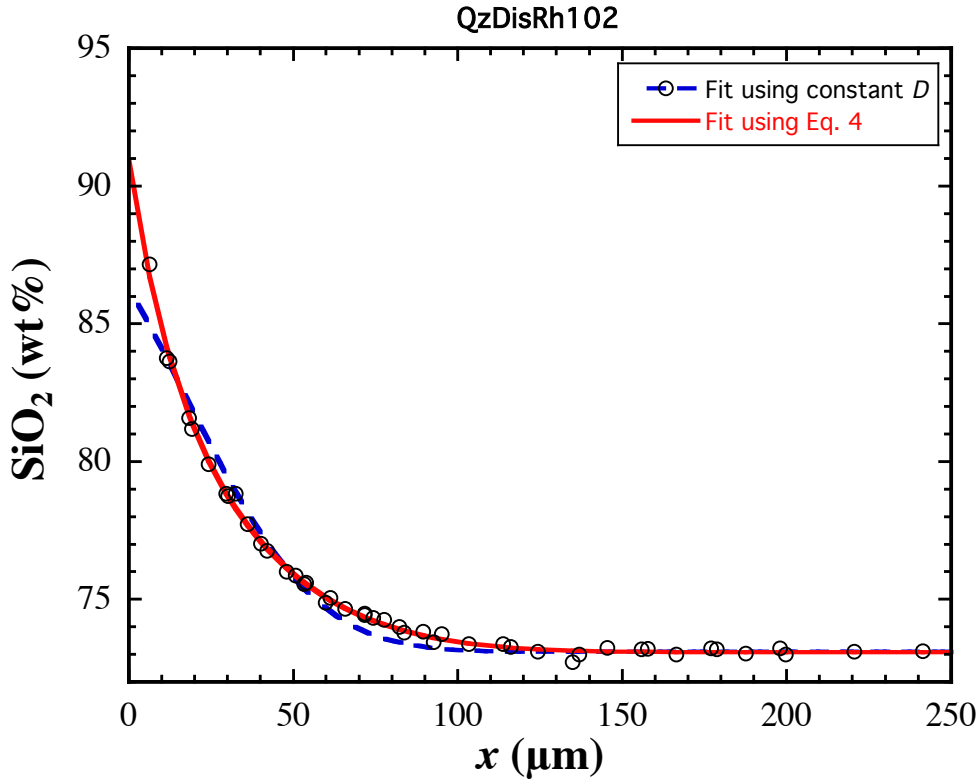

QzDisRh104

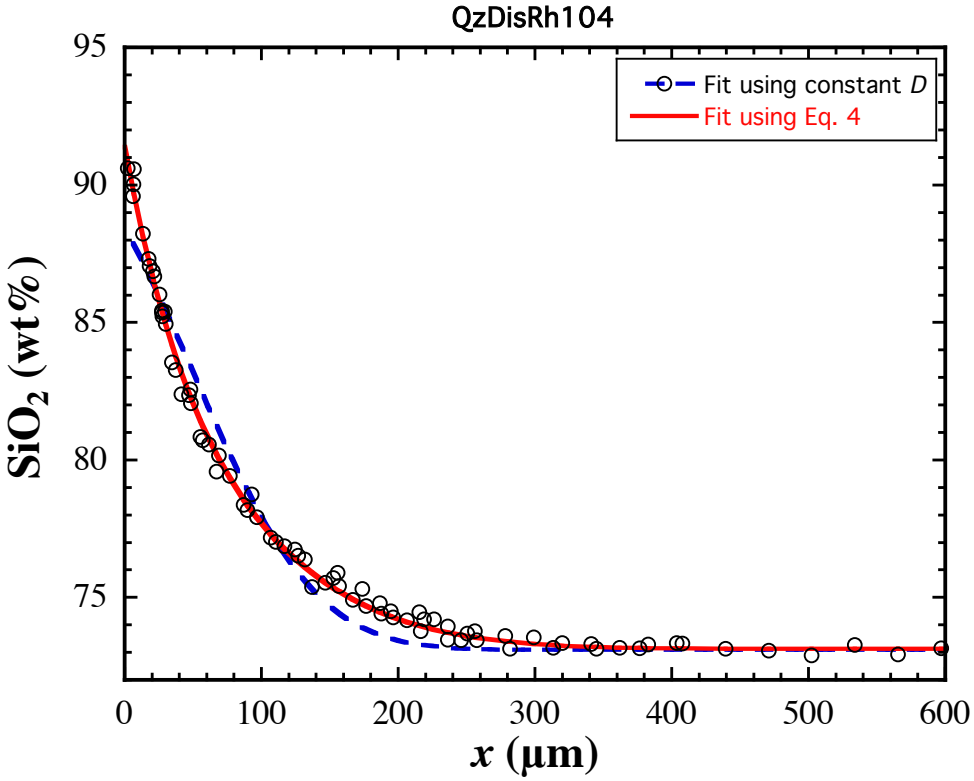

QzDisRh106

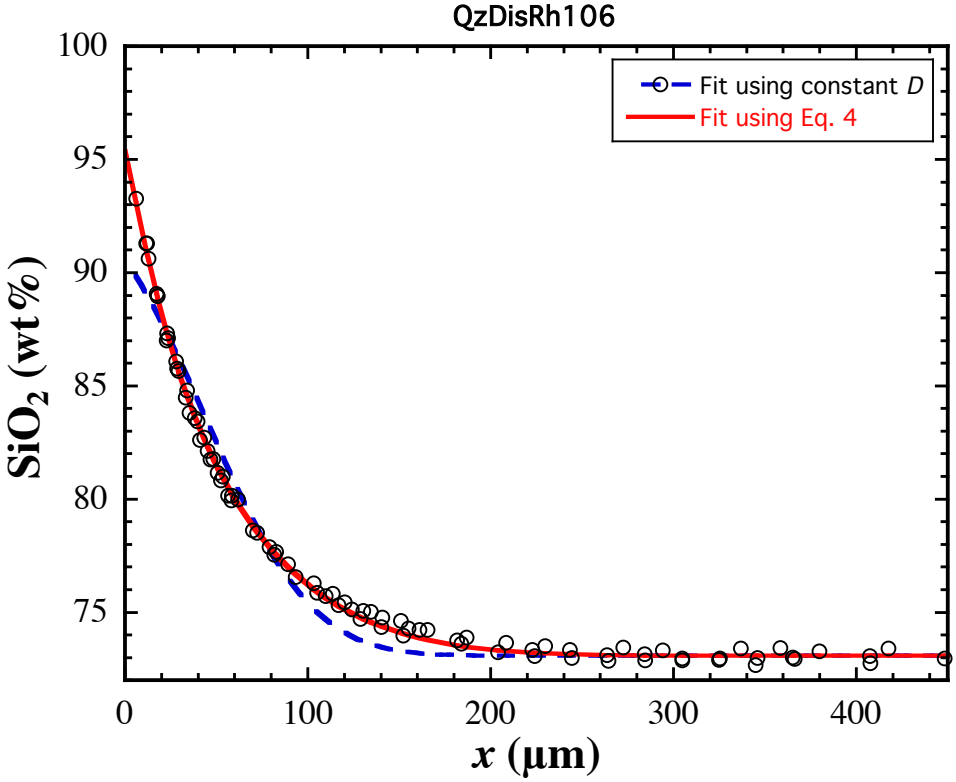

QzDisBa101

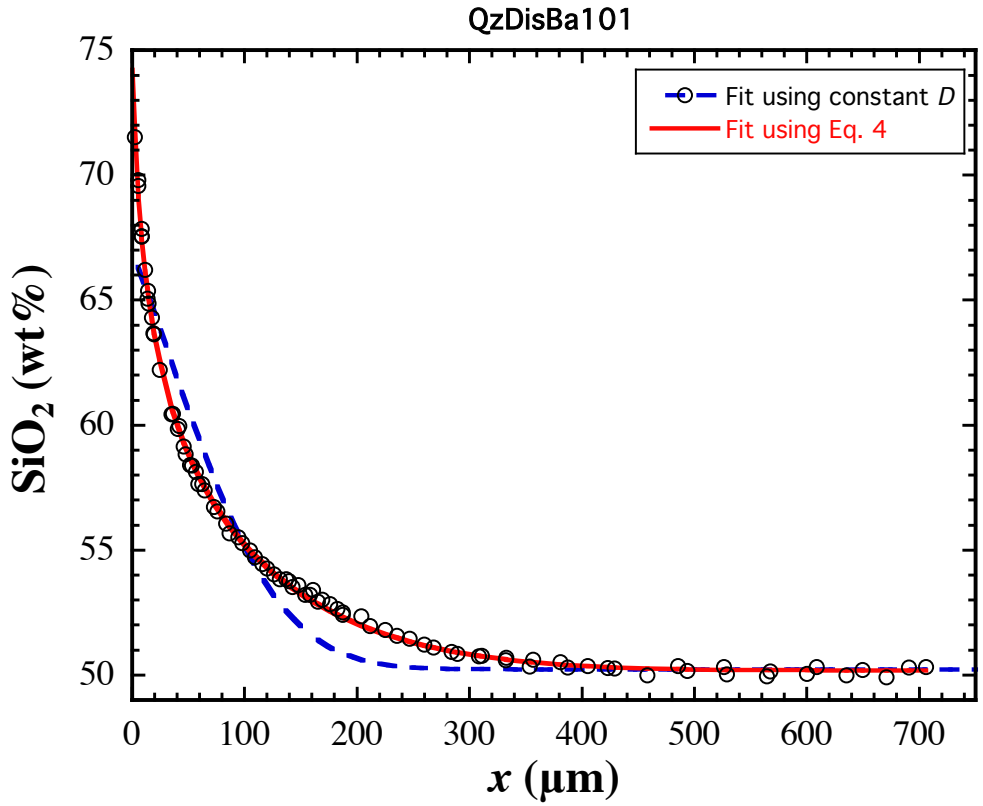

QzDisBa102

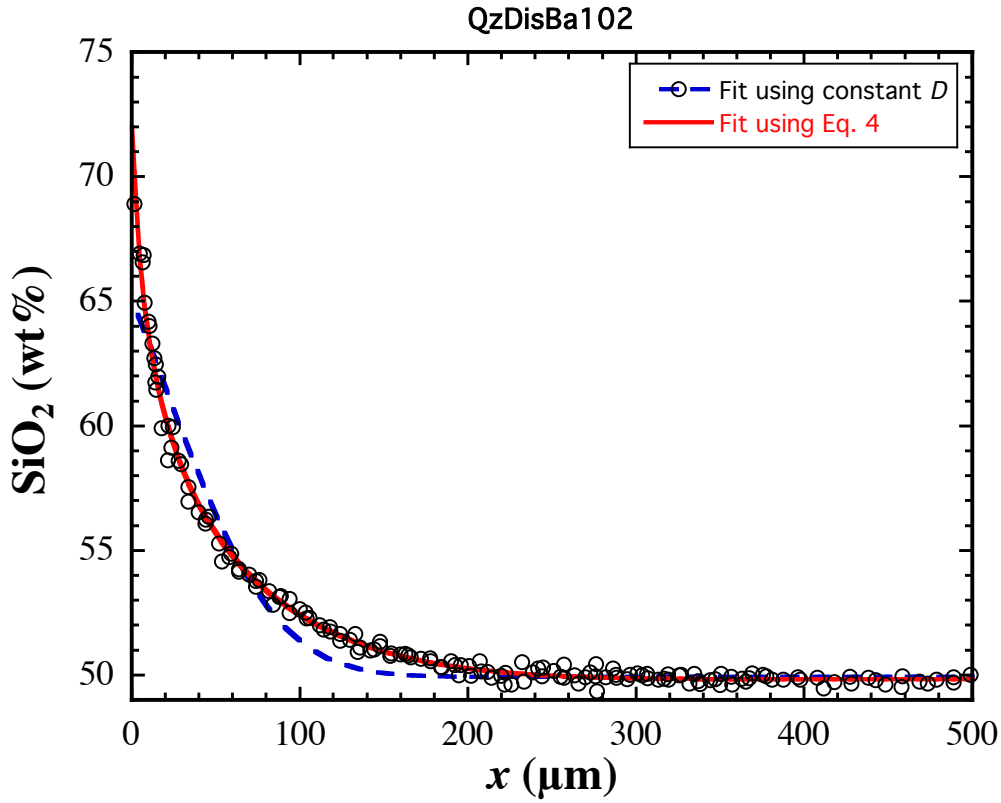

QzDisBa103

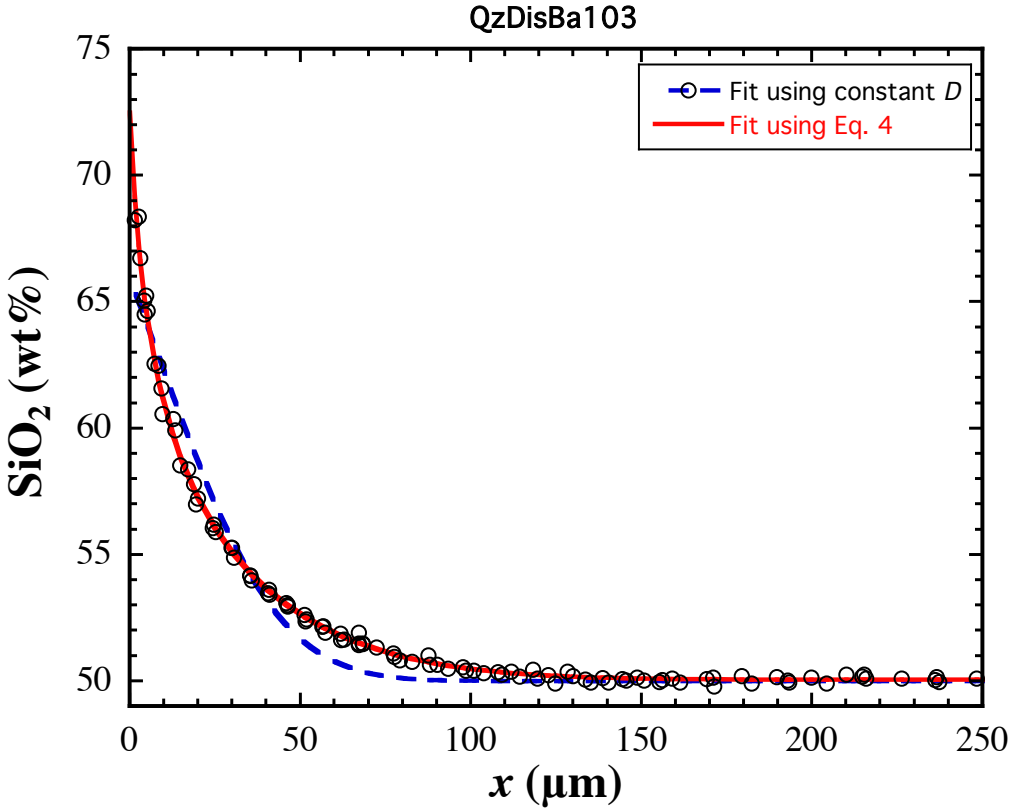

QzDisBa110

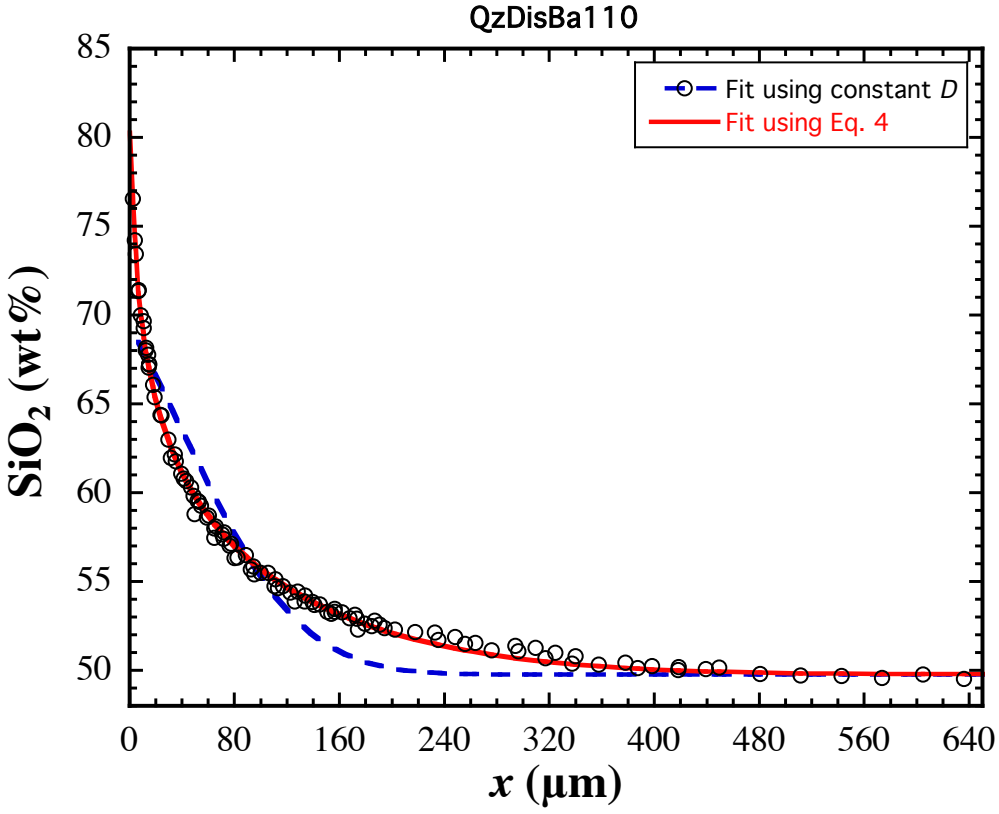

QzDisBa111

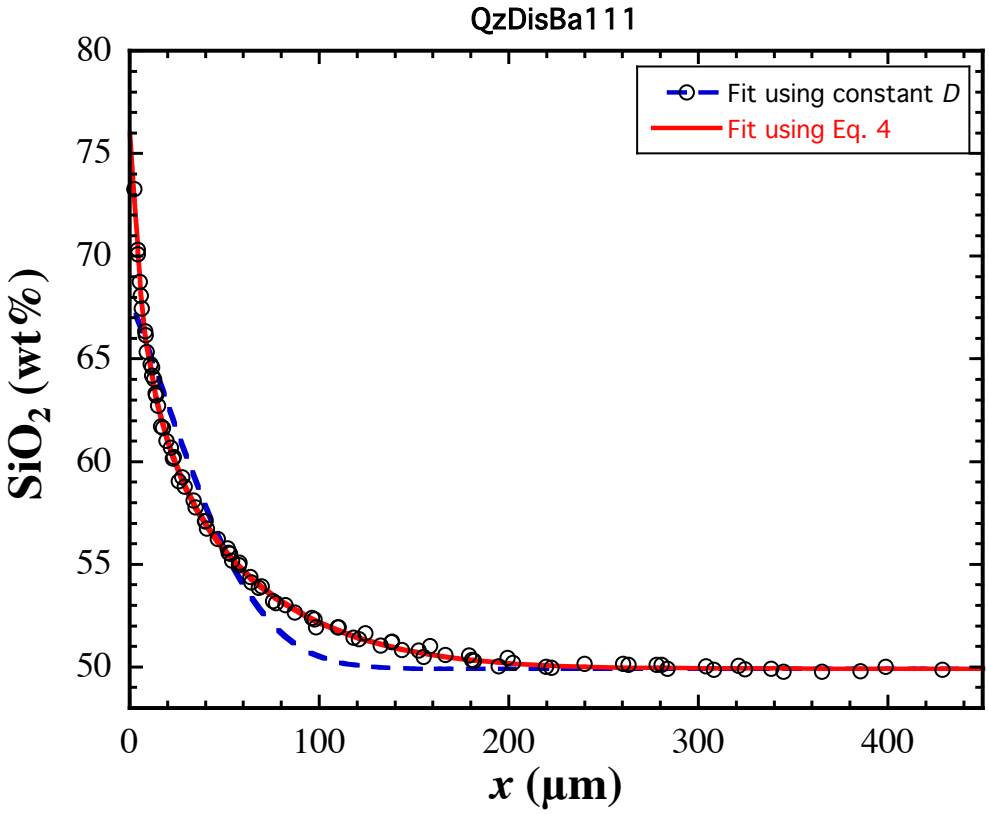

QzDisBa104

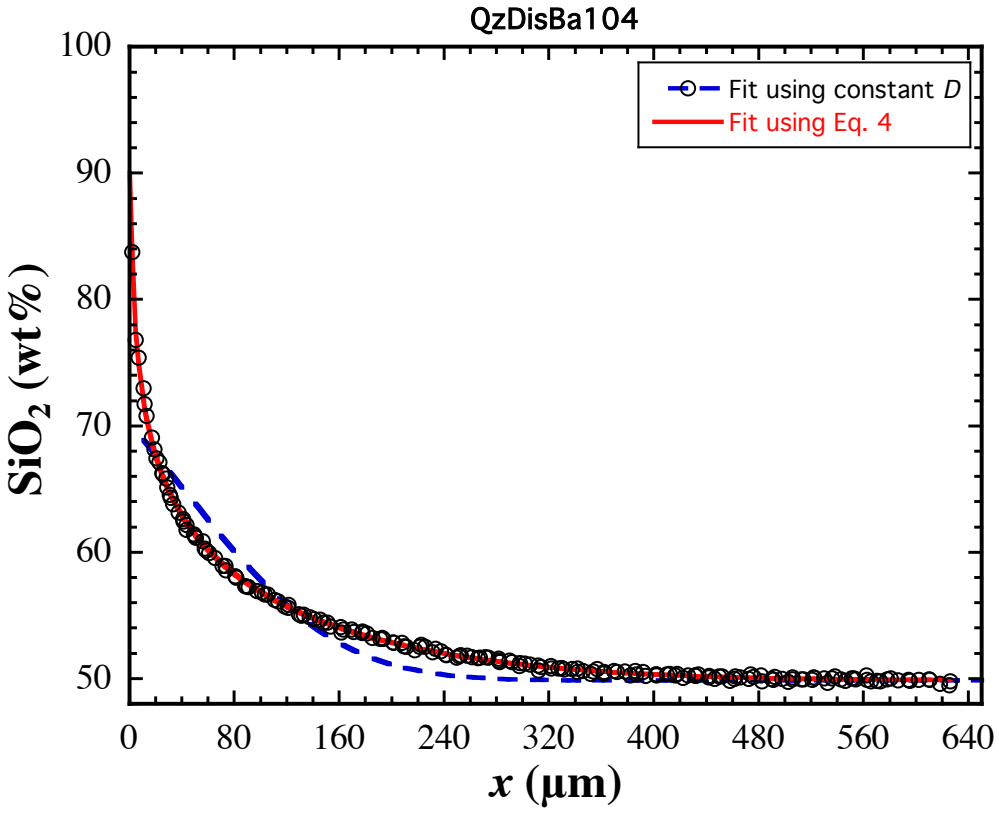

QzDisBa107

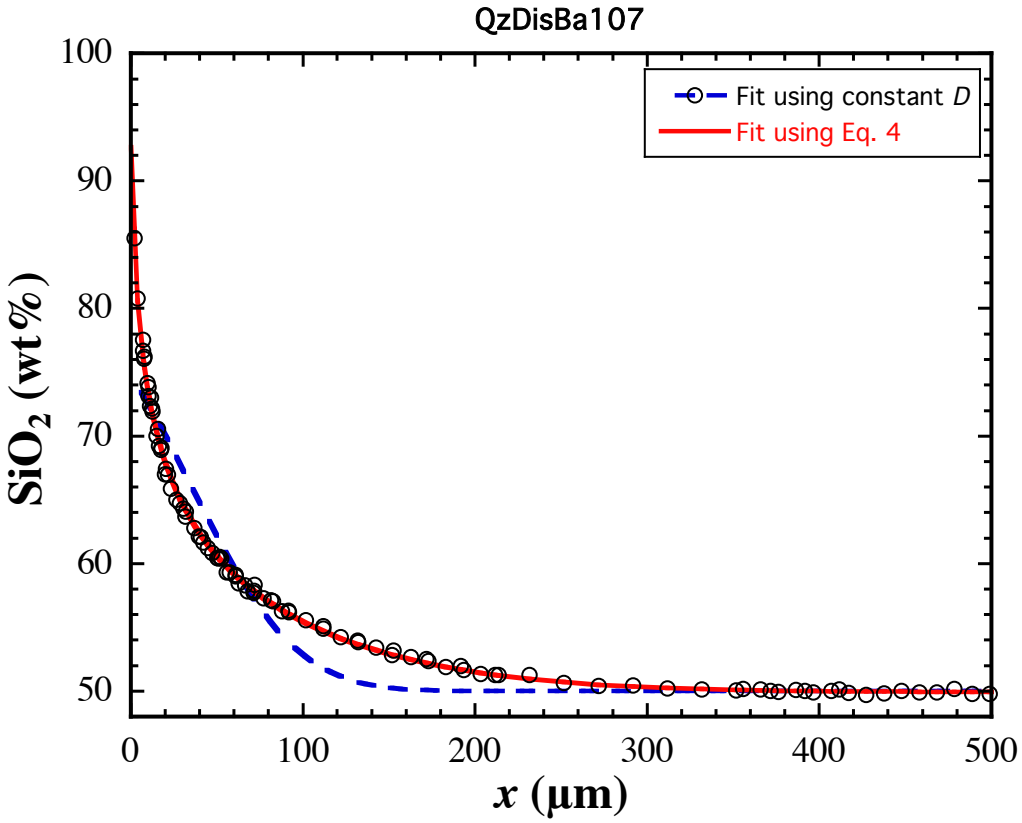
QzDisBa107
Fit using constant D
Fit using Eq. 4
100
90
80
70
60
50
0
100
200
300
400
500
SiO2 (wt%)
x (µm)